Journal Pre-proof

The elastic properties and deformation mechanisms of actin filament networks crosslinked by filamins

Xiaobo Wang, Hanxing Zhu, Yongtao Lu, Zuobin Wang, David Kennedy

Please cite this article as: Wang, X., Zhu, H., Lu, Y., Wang, Z., Kennedy, D., The elastic properties and deformation mechanisms of actin filament networks crosslinked by filamins, *Journal of the Mechanical Behavior of Biomedical Materials* (2020), doi: https://doi.org/10.1016/j.jmbbm.2020.104075.

This is a PDF file of an article that has undergone enhancements after acceptance, such as the addition of a cover page and metadata, and formatting for readability, but it is not yet the definitive version of record. This version will undergo additional copyediting, typesetting and review before it is published in its final form, but we are providing this version to give early visibility of the article. Please note that, during the production process, errors may be discovered which could affect the content, and all legal disclaimers that apply to the journal pertain.

The elastic properties and deformation mechanisms of actin filament networks crosslinked by filamins

Xiaobo Wang [a], Hanxing Zhu [a, *], Yongtao Lu [b], Zuobin Wang [c] and David Kennedy [a]

[a] School of Engineering, Cardiff University, Cardiff, CF24 3AA, UK

[b] State Key Laboratory of Structural Analysis for Industrial Equipment, Dalian University of Technology, Dalian, 116024, China

[c] International Research Centre for Nano Handling and Manufacturing of China, Changchun University of Science and Technology, Changchun, 130022, China

* Email: zhuh3@cardiff.ac.uk

Abstract:

As a substructure of cell cytoskeleton, the crosslinked actin filament networks (CAFNs) play a major role in different cell functions, however, the elastic properties and the deformation mechanisms of CAFNs still remain to be understood. In this paper, a novel three-dimensional (3D) finite element (FE) model has been developed to mimic the mechanical properties of actin filament (F-actin) networks crosslinked by filamin A (FLNA). The simulation results indicate that although the Young's modulus of CAFNs varies in different directions for each random model, the statistical mean value is in-plane isotropic. The crosslinking density and the actin filament volume fraction are found to strongly affect the in-plane shear modulus of CAFNs. The simulation results agree well with the relevant experimental results. In addition, an L-shaped cantilever beam model has been developed for dimensional analysis on the shear stiffness of CAFNs and for quantifying the deformation mechanisms. It has been demonstrated that the in-plane shear modulus of CAFNs is mainly dominated by FLNA (i.e., cross-linkers), and that the bending and torsion deformations of FLNA have almost the same contribution to the stiffness of CAFNs. It has also been found

that the stiffness of CAFNs is almost insensitive to the variation of the Poisson's ratios of FLNA and actin filament in the range from 0.29 to 0.499.

Keywords: crosslinked actin filament networks, modelling, elastic properties, dimensional analysis

1. Introduction

As a ubiquitous intracellular architecture in eukaryotic cells, cytoskeleton plays a crucial role in maintaining the cell shape and bearing external loads. It is mainly composed of three distinct components, i.e., microtubules, intermediate filaments and actin filaments. Among the three components, actin filaments mainly locate just beneath the cell plasma membrane and can form a thin film network which is also known as cell cortex [1]. It surrounds the intracellular domain and can sensitively respond to the external physical or chemical signals. In addition, actin filaments can be crosslinked into other composite structures by different actin binding proteins (ABPs). For example, actin filaments can form lamellipodia, filopodia, stress fibres and contractile rings with different configurations to support or enable specific cell functions [2]. These complex structures always show distinct mechanical properties when participating in different cell functions (e.g., cell motility [3], cell differentiation [4] and cell division [5, 6]). Thus, studying the mechanical responses of cytoskeleton and its substructure becomes more and more imperative and important [1, 7, 8].

During the past decades, both *in vivo* and *in vitro* experiments [9-15] have been conducted to measure the mechanical properties of CAFNs. However, conducting experiments is time-consuming and very expensive, and external conditions can significantly affect the experimental results. Thus, theoretical [16-23] and computational [24-30] models have also been developed to study the mechanical properties of CAFNs. When it comes to the methods

of numerical simulation, FE models and molecule dynamic (MD) models are widely used in studying the mechanical responses (e.g., elastic modulus, Poisson's ratio and stress strain relationship) of CAFNs. As MD models focus on the molecule structure of the polymer chains, they can precisely capture the mechanical responses at the scale of molecule or atom. However, this can cause much more extra costs in computation due to the extreme complexity and large scale of the model. In FE models, filaments and cross-linkers could be simply modelled by elastic beams and assembled into a network structure, which can greatly improve the computational efficiency and reduce the cost. In addition, it is easy to control the network geometry and the material parameters in FE models.

Considering the extreme complexity of these networks and the computation limits, numerical simulations based on representative volume element (RVE) have been conducted because of their advantages in computational efficiency. During the past decades, both two dimensional (2D) models [24-26, 28, 31] and three dimensional (3D) models [29, 30, 32-36] have been developed to probe the mechanical responses of CAFNs. Head et al. [24, 37] studied the elastic responses and deformation modes of crosslinked semi-flexible biopolymer networks by constructing a 2D network model, and all of the intersections (i.e., cross-linkers) were treated as rigid connections in their models. The same treatment for cross-linkers was also adopted by Wilhelm et al. [25], Onck et al. [26] and Bai et al. [31]. Thus, their models have ignored the compliant nature of the actin-binding proteins with a large contour length. Sharma et al. [38] built-up a 2D filamentous network model in which a wormlike chain cross-linker was inserted to represent the connection of two distinct filaments. Recently, Wei et al. [28] developed a 2D network model to study how the physical properties of cross-linker affect the mechanical responses of biopolymer networks, where a linear spring and a rotational spring were inserted at the intersection point of two distinct filaments. In physiological conditions, CAFNs always appear as 3D structure with in-plane periodicity.

Therefore, 3D models are more reasonable than 2D models in mimicking the mechanical responses of CAFNs. Cyron et al. [33] introduced a simulation framework to investigate various biopolymer networks (e.g., isotropic, bundle, cluster and layer network phase) by developing finite element models which could capture the viscoelastic behaviors of the networks and have advantages in efficiency than earlier published models. In their model, actin filaments are randomly distributed and stochastically undulated to represent the thermal equilibrium configuration of actin filament networks. In addition, the friction coefficients of crosslinkers are also introduced in their model. Heidemann et al. [34] investigated the elastic properties of a 3D network that consists of rigid filaments and flexible cross-linkers, where the cross-linkers were modelled as wormlike chains. Ma et al. [39] studied the mechanical behaviour of a 3D fibre-network model where the fibres were modelled by beam elements and the cross-linkers were represented by additionally inserted beam elements. Lin et al. [35] constructed a 3D RVE model to study the active stiffening behaviour of CAFNs by inserting cross-linkers and myosin-II motors at proper positions. These numerical models can help us to investigate the mechanical properties of CAFNs, however, the precise physiological geometry of filamin A (FLNA) has not been taken into consideration. Kim et al. [36] analysed the viscoelastic properties of actin filament networks crosslinked by different actin crosslinking proteins by performing Brownian dynamics simulations on a 3D actin network model which considered the crosslinking angles between two actin filaments. This provides a good reference for the construction of models for crosslinked actin filament networks. In addition, using the correct mechanical properties of actin filament and FLNA is essential in finite element method (FEM) simulations. The mechanical properties of a single actin filament [40-42] and the force-extension relationship of a single FLNA [43] have well been documented. To the best of our knowledge, the effects of components' contents and properties on the elastic properties of CAFNs remain to be understood, especially the effects

4

of some crucial parameters. Therefore, it is necessary to develop new models that can better reflect the physiological conditions (e.g., the realistic geometry, contents and mechanical properties of the building components) of CAFNs.

Due to the page limit, this paper is mainly focused on the linear elastic properties and deformation mechanisms of actin filament networks crosslinked by FLNA, and their nonlinear elastic and viscoelastic properties will be investigated in a separate paper. A three-dimensional actin filament network model is developed to represent the physiological geometry of actin filaments and FLNA using finite element analysis software ABAQUS (Simulia, Providence, RI). By varying the components' contents (i.e., actin filament volume fraction and crosslinking density) and material properties (i.e., Young's moduli and Poisson's ratios), different mechanical responses of CAFNs can be obtained via finite element simulations. This model can precisely capture the elastic properties of CAFNs and reveal the role of CAFNs in different cell functions. In addition, a dimensional analysis is conducted to de-couple and to quantify the contributions of different deformation mechanisms to the stiffness of CAFNs. The details of the model construction and the boundary conditions are elaborated in Section 2; the elastic properties of CAFNs are presented and discussed in Sections 3; the dimensional analysis of CAFNs is presented in Section 4; and the conclusions are summarized in Section 5.

2. Modelling

2.1. Network geometry and parameters

In order to study the elastic properties of crosslinked actin filament networks, a 3D network model is developed using finite element analysis software ABAQUS (Simulia, Providence, RI) and scripting Python, and it shows good consistency with the structure of

actin filament network in electron microscopy images (**Fig. 1**). According to the physiological geometries of cell cortex, actin filaments and FLNA, a periodic representative volume element (RVE) is constructed with a size of $W \times W \times H$, where W is the side dimension and H is the thickness (**Fig. 2**). It is reported that the majority of actin filaments in cell cortex have a physiological length less than 2 μm [11, 44, 45]. The thickness of cell cortex is reported to vary from 0.1 μm to 0.5 μm in different parts of the cell [46], for example, the average thickness of cell cortex in mitotic HeLa cells is measured to be 0.2 μm [47]. Huisman et al. [29] used a 3D model with a size of 2.5 μm to study the mechanical behaviour of CAFNs, in which the length of the actin filaments was between 0.5 μm and 2.0 μm. Chugh et al. [48] developed a 3D plate-like model to investigate the cell surface tension, and their model had a side length of 2.5 μm with the actin filament length ranging between 0.2 μm and 0.8 μm. Gong et al. [49] constructed a three dimensional model (2 μm ×2 μm ×2 μm) to investigate the mechanical responses of a crosslinked biopolymer network, and the filaments in their model had a contour length of 1.2 μm. According to the dimensions of the aforementioned models [29, 48, 49], dimensions W=2 μm and H=0.5 μm are adopted for the RVE models of CAFNs in this work. The constructed geometrical model of CAFNs in **Fig. 1** shows great similarity with the microstructure of crosslinked actin filament networks in living cells.

(a)   (b)

(c)
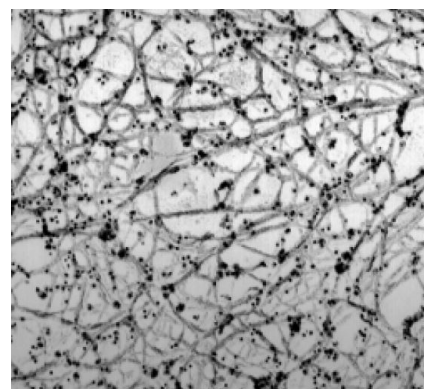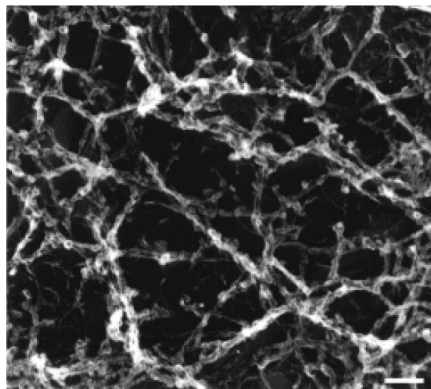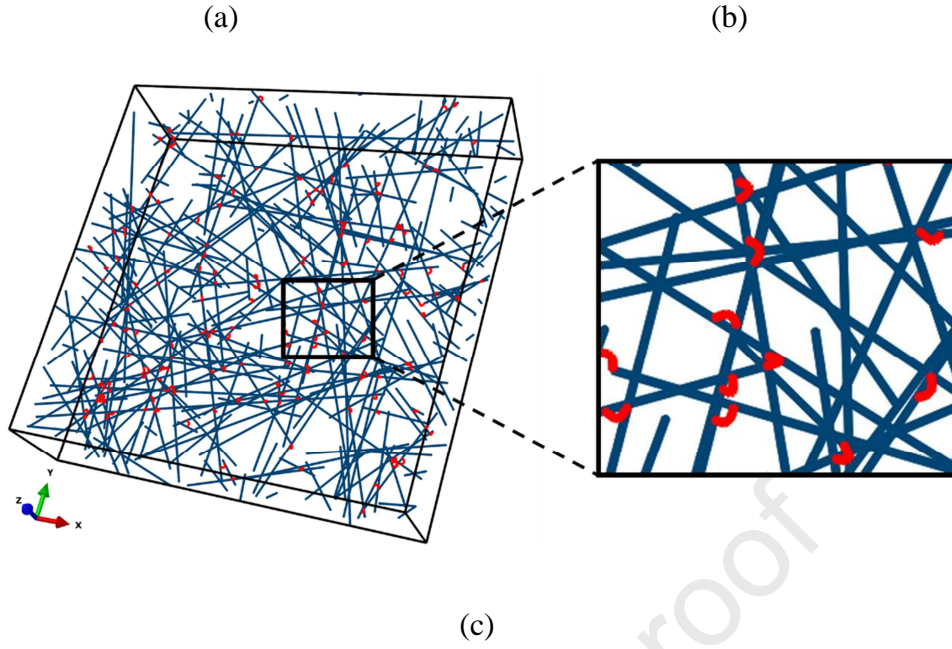
Fig. 1. (a) Electron micrograph of actin filaments crosslinked by FLNA (the bar is 100 nm) [50]. (b) Electron micrograph of actin filament network in human blood platelet [50]. (c) The constructed 3D network model of CAFNs consisting of actin filaments (blue) and FLNA (red).

Actin filaments are usually assumed to have the same length in simulations [24, 33, 48], however, it seems that this treatment neglects the real length distribution of actin filaments in living cells. It is reported that the length of actin filaments approximately holds an exponential distribution when polymerized in *vitro* [51, 52], and similar phenomenon is also observed in eukaryote [44]. In addition, experimental measurements show that the mean length of actin filaments in a whole cell is about 4.9 μm [53]. According to these reports, the length distribution of all filaments in a whole cell can well be described by an exponential probability density function given as [31]

$$f(l,\lambda) = \begin{cases} \lambda e^{-\lambda l}, l \geq 0 \\ 0, \quad l < 0 \end{cases}, \tag{1}$$

where l denotes the length of the individual actin filament and λ^{-1} is the mean length of all actin filaments. It is noted that the probability density function of actin filament lengths (Eq. (1)) is obtained for all the actin filaments in a whole cell [44], and that most actin filaments in the cell cortex are shorter than 2 μm [11, 44, 45]. In addition, FLNA tends to associate with actin filaments which are longer than 50 nm according to the binding mechanisms [54]. Thus, only actin filaments with a length between 0.05 μm and 2 μm are generated in the RVE model (the shaded region in **Fig. 2** (b)), and their mean length can be obtained as

$$L_m = \sum_{i=1}^{N} l_i \Big/ N , \qquad (2)$$

where N is the total number of complete actin filaments generated in the RVE model and l_i is the length of filament i. It is worth noting that actin filaments with the length of 4 μm are generated in a cubic volume of edge length of 5 μm in the computational model proposed by Cyron et al. [33], which is different from our model in the dimensions of RVE and length distribution of actin filaments. In addition, the thermal fluctuation of actin filaments as well as the friction of crosslinkers are taken into consideration in Cyron's model [33], however, these factors are not included in our model.

To generate a filament in a RVE, the x, y and z coordinates of its midpoint are determined by random numbers in the space of $W \times W \times H$. α is defined as the angle of turning the filament projection on the x-y plane (l_{xy}) clockwise to the positive direction of the x axis. As actin filaments are randomly oriented on the x-y plane of the RVE, α is randomly determined in the range of 0 to π. β is defined as the angle between the filaments and the x-y plane. It is worth noting that some filaments have a length larger than the thickness H of the RVE, while the others have a length smaller than H. When the length of a filament is smaller than H, β is randomly determined in the range of 0 to $\pi/2$. If the length of a filament is larger than H, an upper limit value for β is defined by

$$\beta_{ul} = \arcsin\left(H/l\right).\tag{3}$$

In this case, β is randomly determined in the range of 0 to β_{ul}. If part of a filament is outside the top or bottom surface of the RVE, the filament is translated in the z direction to the position with its top end on the top surface or its bottom end on the bottom surface of the RVE, as shown in **Fig. 2** (d). In addition, all filaments generated in the central REV are copied to the neighbouring 8 RVEs, thus periodic boundary conditions can be achieved in the x and y directions, as demonstrated in Fig. 2(c).
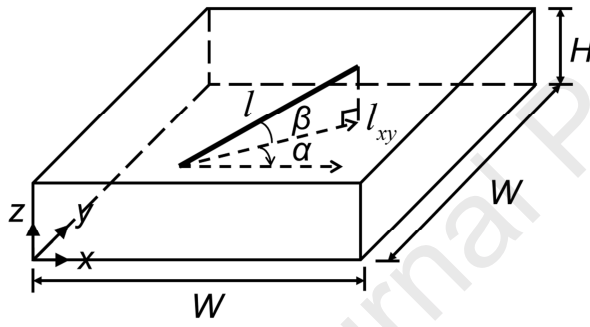
(a)
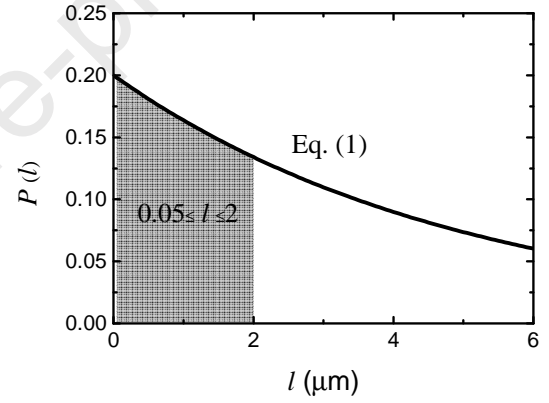
(b)
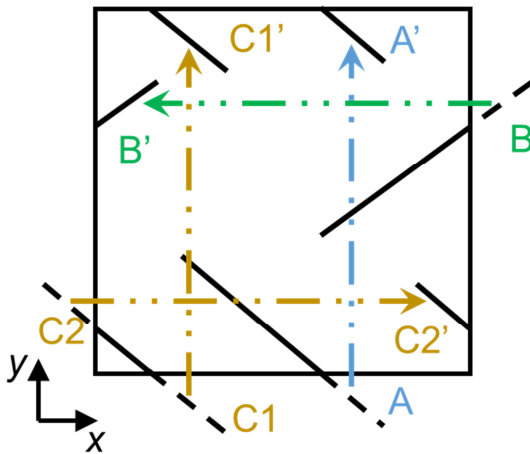
(c)

(d)

Fig. 2. The construction details of actin filaments in RVE: (a) the position and orientation of a filament in RVE; (b) the length distribution of the actin filaments in the RVE model of CAFNs; (c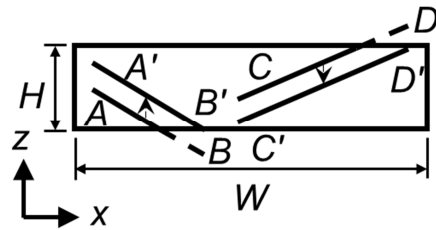) the diagrammatic sketch of how to keep periodicity of RVE in the *x* and *y* directions; (d) the method of processing out-of-plane protrusions of a filament.

The Young's modulus of actin filaments E_f is measured to be about 2 GPa [40-42], and the cross-sectional area A_f is about 20 nm^2 [40, 41]. Thus, a circle cross section with a radius of 2.52 nm is adopted for the actin filaments in our model. To the best of our knowledge, we are not aware of any experimental work that has actually measured the Poisson's ratio of a single actin filament, however, an estimated or calculated Poisson's ratio of about 0.3 to 0.4 is used for modelling or studying the actin filaments in previous studies [35, 55, 56]. Therefore, an average value of 0.35 is adopted as the Poisson's ratio of actin filaments in our model. For simplicity, cross-linkers are also represented by elastic rods with specific geometric and material properties. Experimental measurements show an axial extension stiffness ($\mu = EA/L$) of FLNA ranging from 5×10^{-4} N·m^{-1} to 1×10^{-3} N·m^{-1} [57], and 2×10^{-4} N·m^{-1} is adopted by Wei et al. [28]. The contour length (l_{cl}) of FLNA dimer is reported to be about 160 nm [54, 58]. Additionally, the radius of the circular cross-section of cross-linkers is estimated to be 1.8 nm according to the microstructure of FLNA [54]. Thus, the Young's modulus of the cross-linkers (E_c) can be obtained as E_c=12 MPa from their axial extension stiffness (μ), cross-sectional area (A_c) and contour length (l_{cl}) of FLNA. The Poisson's ratio of cross-linkers is simply assumed to be the same as that of actin filament in this paper. **Table 1** shows the material properties and cross-sectional dimensions of actin filaments and FLNA which are adopted in our models of CAFNs. It worth noting that the FLNA dimers are represented by their rod 2 segment in simulations, which are illustrated in Section 2.2. The rod 2 segment of FLNA has the same material properties and cross-section with FLNA dimer,

however, the total length of the rod 2 segment in a single FLNA dimer is about 40 nm (**Fig. 3** (a)).

Table 1

The material properties and dimensions of actin filament and FLNA in simulations.

Components	Young's modulus (Pa)	Poisson's ratio	Cross-sectional type	Cross-sectional radius (nm)	Cross-sectional area (nm^2)
Actin filament	2.3E+09	0.35	circle	2.52	19.95
FLNA	1.2E+07	0.35	circle	1.80	10.18

According to the geometric parameters determined above, the volume fraction of actin filaments, V_f, can be specified as

$$V_f = \frac{\sum_{i=1}^{N} l_i \times A_f}{W \times W \times H} \,. \tag{4}$$

2.2. Crosslinking principles

FLNA is a type of actin-binding proteins that can bind distinct actin filaments into an orthogonal network structure. As FLNA has a relatively large contour length (approximately 160 nm) and an easily deformable "*V*" shape [54, 58], cross-linkers (i.e., FLNA) between two distinct filaments are modelled by deformable curved elastic rods. In addition, the angle at the FLNA dimerization point is reported to range from 60° to 120° with an average angle being about 90° [54]. According to the microstructure of FLNA and its interaction with actin filaments [54, 58, 59], two filaments are crosslinked only when their crossing angle (θ_c) is

11

larger than 60° and smaller than 120°, and their distance (d_c) is smaller than 35 nm (approximately the distance between two terminals of the rod 2 segment in a FLNA dimer when the angle at the dimerization point is 120º). In order to guarantee the uniformity of crosslinking, only one cross-linker is inserted between each pair of actin filaments until the expected crosslinking density is reached. If the crosslinking density is still smaller than the expected value when all of the available crosslinking points are crosslinked by one cross-linker, the cross-linker generation process will be repeated until the expected crosslinking density is reached. This means that some pairs of actin filaments are crosslinked by more than one cross-linker. It is noted that actin bundles can be formed in the reconstituted actin filament networks crosslinked by filamins when the crosslinker concentration is at very high level [60, 61]. Different types of network structures (e.g., homogeneous-isotropic networks, bundles, clusters and layers) can be formed by changing the concentrations of actin filaments and crosslinkers as well as the orientation constraints of crosslinking in the computational model proposed by Cyron et al. [33]. Due to the fact that the crosslinking density studied in this research is not very high, the mechanism of forming actin bundles is not taken into consideration in our model. But the adoption of deformable "*V*" shaped crosslinkers in our model could better reflect the real contour of FLNA in living cells.

As this paper is mainly focused on the linear elastic properties (i.e., small strain stage) of crosslinked actin filament networks, the unbinding between FLNA and actin filaments is ignored. Therefore, the binding points between FLNA and actin filaments are simply treated as permanently shared nodes (i.e., both FLNA and actin filaments have the same displacements and rotations at their shared nodes). As the total length of the rod 2 segment is 40 nm, a specific distance of 35 nm is used as the critical distance for crosslinking. It is easy to find that large crossing angles tend to appear more frequently than smaller ones, which

may explain the reason why FLNA prefers to crosslink actin filaments into orthogonal connections. **Fig. 3** shows the crosslinking mechanism.

The crosslinking density (i.e., the mean number of cross-linkers per micron length of actin filament), ρ_c, is defined as the connectivity of crosslinked actin filament networks and given by

$$\rho_c = n_c / L_t \, , \tag{5}$$

where n_c and L_t refer to the total number of cross-linkers and the total length of actin filaments in the RVE model, respectively. In experiments, the connectivity of the network is always controlled by tuning the molar ratio of FLNA dimers to actin monomers (R_F). Experimental results showed that 0.2 μm long actin filament contains about 76 subunits of actin monomers[44], from which we can obtain the equivalent molar ratio of FLNA to actin in our model as $R_F = \rho_c / 380$. In living cells and *in-vitro* experiments, it is proved that binding and unbinding between filaments and FLNA take place all the time. Under such a circumstance, some actin filaments are crosslinked by more than one cross-linker although some actin filaments may not be crosslinked. Once some actin filaments are crosslinked into a continuum path throughout the RVE, loads applied to the network can be transmitted. Although some of the actin filaments are not crosslinked at all (i.e., isolated), they are also included when calculating the nominal volume fraction of actin filaments (V_f) in Eq. (4). Only in this way, is the definition of the nominal volume fraction of actin filaments in this work consistent with the fact in experiments.

(a)

(b)

(c)
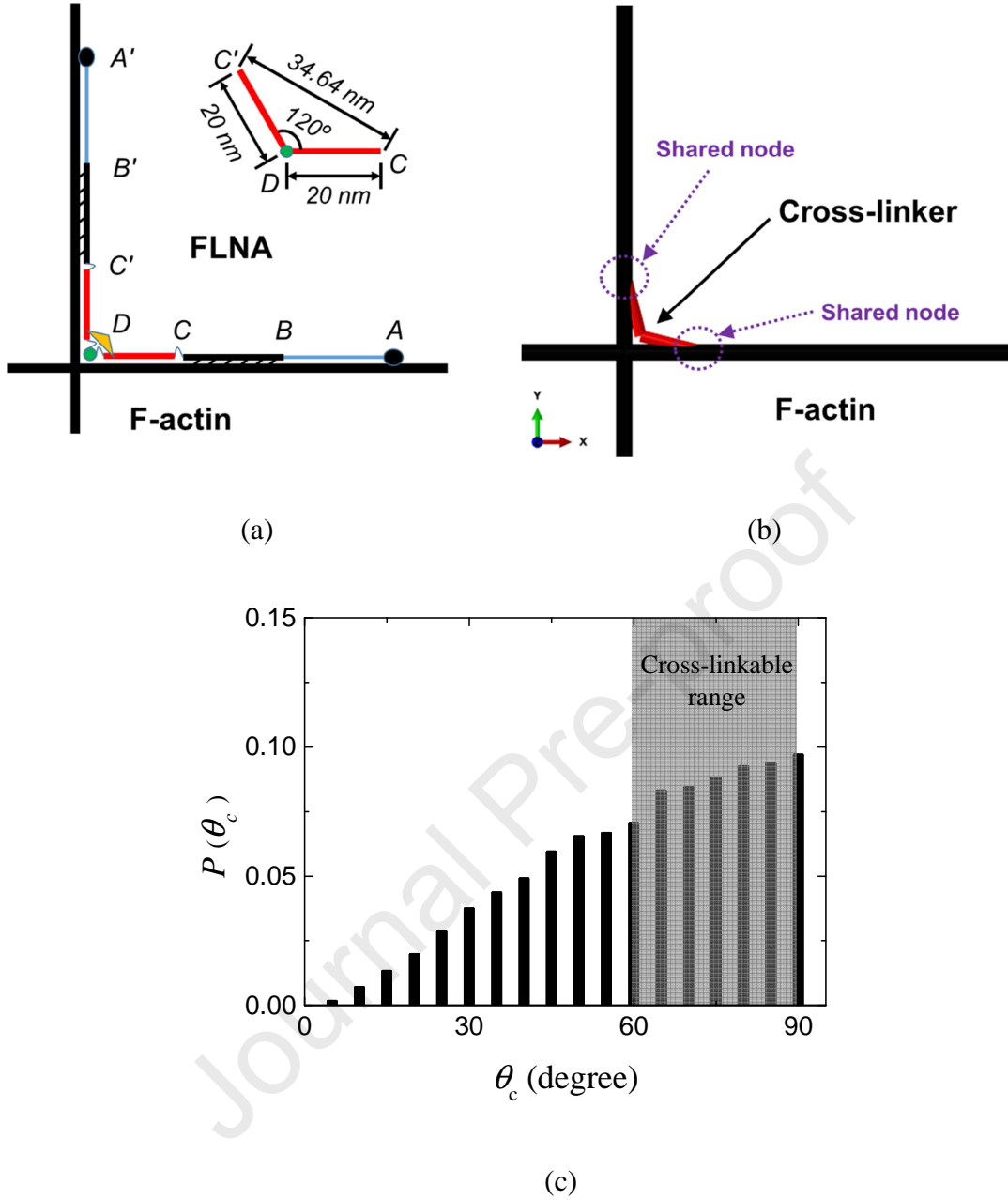
Fig. 3. (a) Diagrammatic sketch of the microstructure of an ideally orthogonal connection formed by FLNA and actin filaments [54, 58]. Where A refers to the actin-binding domain (black solid point), AB refers to Ig1-8 of FLNA which does not bind with actin filament, BC refers to Ig9-15 of FLNA that binds with actin filament, C refers to Hinge-1 of FLNA, CD refers to Ig16-23 of FLNA which is also known as rod 2 segment, D refers to the dimerization (green solid point), the yellow solid triangle is FilGAP: a FLNA-binding RhoGTPase-activating protein. The inset shows the geometric details of rod 2 segment when the crosslinking angle is 120 degree, which determines the critical distance for crosslinking.

14

(b) The details of a cross-linker (in red) generated in our model. Because BC and B'C' (Ig9-15) are assumed to bind with actin filament permanently in our model, only CD and C'D (Ig16-23) are presented in FE model. (c) The statistical results of probability distribution of the crossing angles (θ_c) between actin filaments in RVEs (over 100 models). The shaded area refers to the range of potential crosslinking angles.

2.3. Mesh and boundary conditions

All of the actin filaments and FLNA in the RVE are meshed into Timoshenko beam elements (B32), which could successfully take into consideration the bending, torsion, axial stretching/compression, and transverse shear deformation of the beam. To mesh the actin filaments, an element size (length) of 0.04 μm is adopted because actin filaments are much longer than FLNA. According to the discussion of crosslinking principles, the FLNA is represented by its rod 2 segment in finite element simulations, and the rod 2 segment (see **Fig. 3** (b)) of each FLNA (i.e. cross-linker) has a total length of $L_c = 0.04$ μm and is meshed into 10 Timoshenko beam elements. For simplicity, both the actin filaments and FLNA are assumed to have a uniform circular cross-section with a constant area as given in **Table 1**. In addition, both actin filaments and FLNA are assumed to be isotropic materials with Young's moduli and Poisson's ratio shown in **Table 1**.

As the RVE model is periodic in the x and y directions, periodic boundary conditions (PBCs) are more suitable for these boundaries [62, 63]. For each pair of nodes on the opposite planes, the PBCs simply assume that they have the same nodal rotations, and the differences of their nodal displacements remain constants in the *x*, *y* and *z* directions. By simply ignoring the interactions between cell cortex and cell plasma membrane, all the nodes on the top and bottom surfaces of the RVE (shown in **Fig. 1** (c)) are left to be free (i.e., these

nodes are free to displace or rotate). These boundary conditions for the nodes on the top and bottom surfaces were also adopted to study the effects of cell cortex structure on cell surface tension in reference [48].

3. Simulation results

3.1. Determination of the elastic constants

The random distribution of the actin filaments in cell cortex indicates that there are three orthogonal planes of elastic symmetry, and in addition, the *x-y* plane is isotropic. Thus, the crosslinked actin filament networks (CAFNs) have only five independent elastic constants [64, 65]. Under small deformation, the stresses of the CAFNs are related to the strains by the following relationship:

$$
\begin{Bmatrix} \varepsilon_{11} \\ \varepsilon_{22} \\ \varepsilon_{33} \\ \gamma_{23} \\ \gamma_{31} \\ \gamma_{12} \end{Bmatrix} = \begin{bmatrix} \dfrac{1}{E_1} & -\dfrac{v_{12}}{E_1} & -\dfrac{v_{13}}{E_3} & 0 & 0 & 0 \\ -\dfrac{v_{21}}{E_1} & \dfrac{1}{E_1} & -\dfrac{v_{13}}{E_3} & 0 & 0 & 0 \\ -\dfrac{v_{31}}{E_1} & -\dfrac{v_{31}}{E_1} & \dfrac{1}{E_3} & 0 & 0 & 0 \\ 0 & 0 & 0 & \dfrac{1}{G_{31}} & 0 & 0 \\ 0 & 0 & 0 & 0 & \dfrac{1}{G_{31}} & 0 \\ 0 & 0 & 0 & 0 & 0 & \dfrac{1}{G_{12}} \end{bmatrix} \begin{Bmatrix} \sigma_{11} \\ \sigma_{22} \\ \sigma_{33} \\ \sigma_{23} \\ \sigma_{31} \\ \sigma_{12} \end{Bmatrix}. \tag{6}
$$

Since the compliance matrix in Eq. (6) is symmetric about the leading diagonal (e.g., v_{31}/E_1 = v_{13}/E_3) and $G_{12} = E_1/2(1+v_{12})$, there are only five independent elastic constants: E_1, v_{12}, E_3, v_{31} and G_{31}. In consideration of the fact that the cell cortex mainly bears in-plane (*x-y* plane) loads (e.g., arterial cell bears shear stress of blood flow [66]) rather than those in the out-of-

16

plane (z direction), only the in-plane elastic properties are studied and presented in this paper. For simplicity, reference points are set up by coupling nodes in corresponding faces of the RVE, and their reaction forces as well as displacements can be obtained from the output database. The effective engineering stress can be obtained as

$$\sigma = F/A , \tag{7}$$

where F is the reaction force of the loaded reference point and A is the effective cross-sectional area of loaded plane. The effective engineering strain can be obtained by dividing the tensile deformation d by the initial side length W of the RVE model, and given by

$$\varepsilon = d/W . \tag{8}$$

In order to study the in-plane elastic properties of the network, a small strain (0.001) is applied to the RVE model. The effective Young's modulus (E) and the Poisson's ratio (v) of the network can be obtained by conducting uniaxial tension simulations and using the periodic boundary conditions.

$$\begin{cases} E_{11} = \sigma_{11}/\varepsilon_{11} \\ v_{21} = -\varepsilon_{22}/\varepsilon_{11} \end{cases} , \tag{9}$$

where σ_{11} is the effective engineering normal stress under uniaxial tension, ε_{11} is the tensile strain in the loading direction, and ε_{22} is the corresponding normal strain in the orthogonal direction. It is noted that the actin filament networks may have been pre-stressed. For small deformation of linear elastic materials/structures, however, the principle of superposition applies, and pre-stress or pre-strain does not affect the results of the linear elastic properties.

3.2. Isotropic properties

The simulation results for 20 random models with a fixed actin filament volume fraction ($V_f = 0.4\%$) and a fixed crosslinking density ($\rho_c = 1.0$) are listed in **Table 2**. As can be seen,

17

although E_{11} is different from E_{22} and v_{12} is different from v_{21} for each of the individual random models, the statistical mean Young's moduli and Poisson's ratios are almost identical in the x and y directions (i.e., $E_{11} = E_{22}$ and $v_{12} = v_{21}$), and $G_{12} = E_{11}/[2(1+v_{12})]$. These results suggest that the CAFNs are in-plane isotropic, because actin filaments are randomly distributed in the x-y plane.
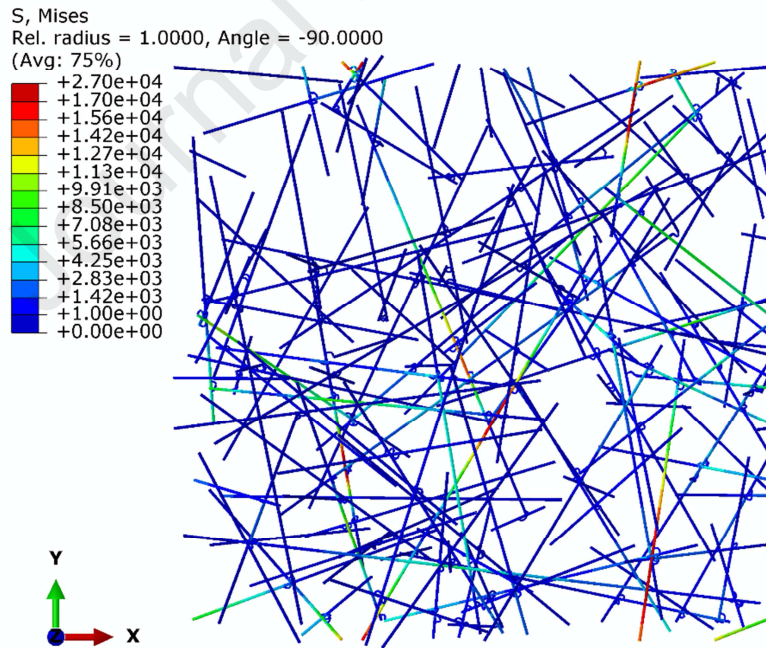
Table 2

The in-plane Young's moduli, Poisson's ratios and shear moduli of 20 periodic random RVE models with a fixed actin filament volume fraction of $V_f = 0.4\%$ and a fixed crosslinking density of $\rho_c = 1.0$.
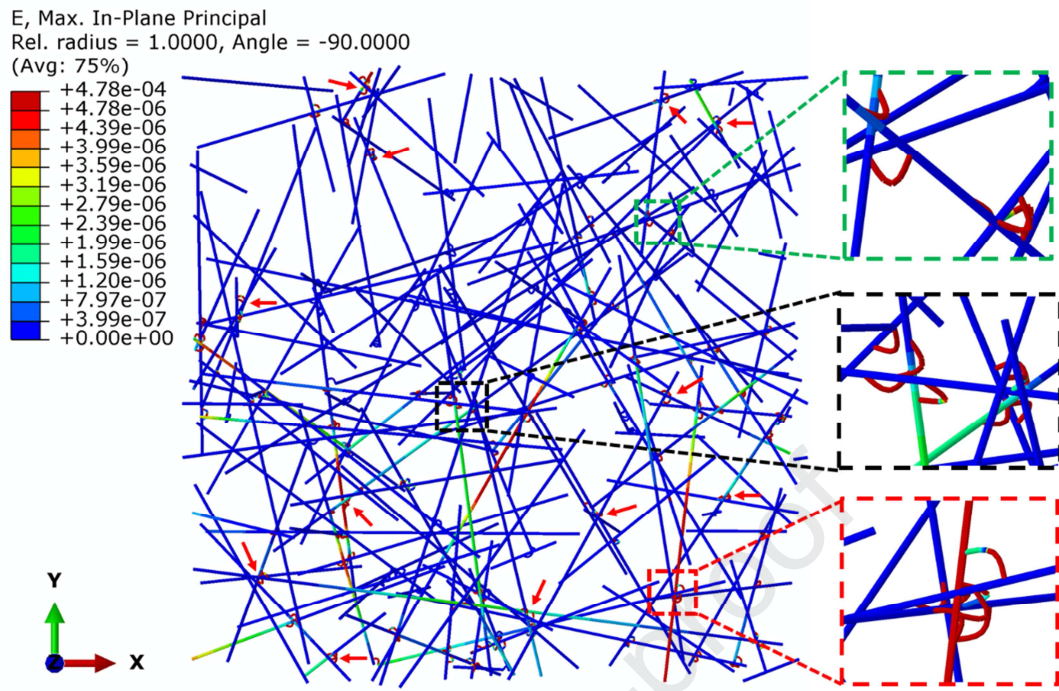
Model No.	E_{11} (Pa)	v_{21}	E_{22} (Pa)	v_{12}	G_{12} (Pa)
1	11.0289	0.1023	11.8114	0.1096	5.1154
2	18.2018	0.2432	28.1523	0.3761	13.8023
3	27.2581	0.0819	24.7734	0.0744	10.5504
4	8.5795	0.0092	7.4726	0.0080	2.4938
5	20.3106	0.3131	12.4534	0.1920	9.8949
6	27.4947	-0.0829	15.2173	-0.0459	4.3915
7	11.2361	0.0907	11.5941	0.0936	3.5636
8	19.1121	0.1014	22.3218	0.1184	11.5540
9	26.0576	0.0163	14.5517	0.0091	9.8759
10	18.1095	0.1671	26.3887	0.2434	7.1442
11	16.8870	0.1359	16.9425	0.1363	6.7550
12	9.8979	0.0545	20.4827	0.1129	3.1596
13	13.9251	0.2178	7.7709	0.1216	3.7496
14	18.3405	0.3085	6.1464	0.1034	7.5101
15	32.1869	0.2359	18.5847	0.1362	10.4478
16	14.8388	0.1350	16.6581	0.1516	9.4976
17	6.9136	0.0223	26.0117	0.0841	5.1805
18	23.8214	0.3038	14.2944	0.1823	11.3357
19	17.4011	0.2277	31.3956	0.4109	10.5491
20	7.2054	0.1364	17.7829	0.3367	6.0938
Mean	17.4403	0.1410	17.5403	0.1477	7.6332
Standard deviation	7.0455	0.1076	7.0225	0.1150	3.2406

As the CAFNs are in-plane isotropic, and most experiments are conducted to measure the shear modulus of CAFNs, shear simulations are performed in the following parts to study the
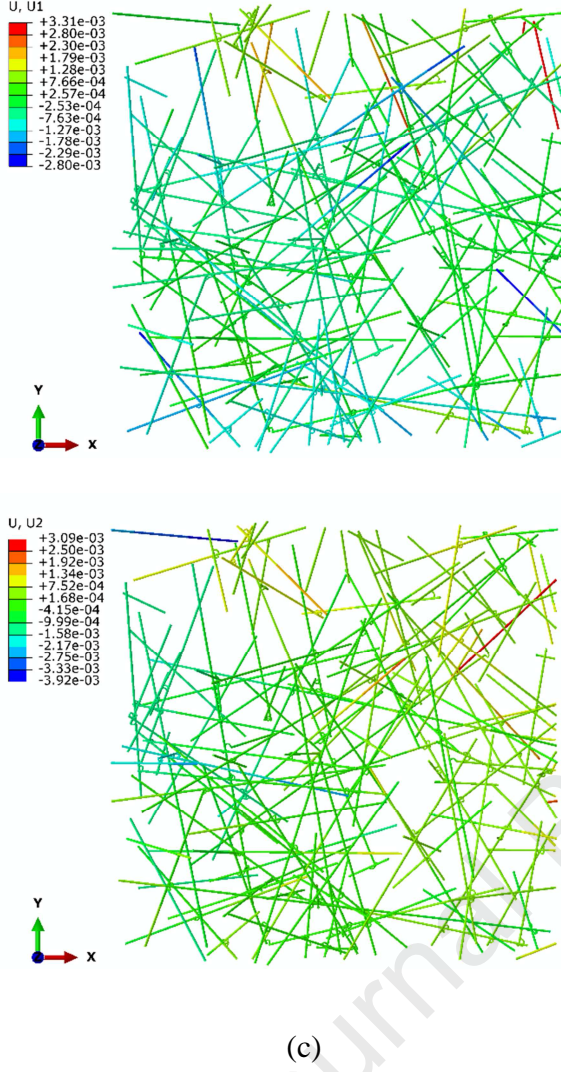
elastic properties of CAFNs. By using periodic boundary conditions and applying a small shear strain (0.001) to the RVE model, the effective shear modulus of RVE can be obtained. The contours of stress distribution, strain and in-plane displacements of the filaments and cross-linkers in the RVE can also be obtained from simulations, as demonstrated in **Fig. 4**. It can be seen from **Fig. 4** (a) that only some of the actin filaments bear the stress in the RVE, and the other actin filaments don't undertake any stress. **Fig. 4** (b) shows that the strain (indicated by red arrows) is mainly concentrated in the cross-linkers rather than in actin filaments, which suggests that the cross-linkers play a dominant role in the deformation mechanism of the CAFNs in small strain stage. **Fig. 4** (c) and (d) present the in-plane displacements in the x and y directions, respectively.

(a)

E, Max. In-Plane Principal
Rel. radius = 1.0000, Angle = -90.0000
(Avg: 75%)
+4.78e-04
+4.78e-06
+4.39e-06
+3.99e-06
+3.59e-06
+3.19e-06
+2.79e-06
+2.39e-06
+1.99e-06
+1.59e-06
+1.20e-06
+7.97e-07
+3.99e-07
+0.00e+00

(b)

20

<div align="center">(c)   (d)</div>

Fig. 4. The von-Mises stress (Pa) distribution (a), maximum in-plane principle strain (b) and

in-plane displacements (μm) in the *x* direction (c) and in the *y* direction (d) of the RVE.

3.3. Effects of actin filament volume fraction and crosslinking density on the in-plane shear modulus of CAFNs

In different cells or distinct regions of a single cell, the volume fraction of actin filaments (V_f) and the crosslinking density (ρ_c) are always different in order to meet the requirements of specific functions. V_f and ρ_c are the two main factors that can significantly affect the elastic properties of CAFNs. In this section, we investigate the effects of V_f and ρ_c on the in-

plane shear modulus of CAFNs. 100 models are simulated for each of the different volume fraction (or crosslinking density) conditions to obtain the statistical results, and the simulation results are presented in **Fig. 5**. As can be seen in **Fig. 5** (a), the simulation results of the in-plane shear modulus, G_{12}, is approximately proportional to $V_f^{5/2}$, which is consistent with the experimental measurements on crosslinked gels [10, 17, 67]. Although strut bending is the dominant deformation mechanism in both low density random irregular Voronoi open-cell foams [62] and honeycombs [63], the shear modulus G_{12} (or Young's modulus) is proportional to V_f^2 for random irregular open-cell foams (3D) [62] and to V_f^3 for random irregular honeycombs (2D) [63]. As the geometrical structure of CAFNs (shown in **Fig. 1** (c)) is somewhat between random irregular Voronoi honeycombs (2D) [63] and random irregular Voronoi open-cell foams (3D) [62], their relationship between G_{12} and V_f is also between those of the two types of cellular materials. The geometries of an undeformed random Voronoi open-cell foam and an undeformed random Voronoi honeycomb are provided in **Fig. 6** for comparing with that of the CAFNs.

Fig. 5 (b) indicates that the in-plane shear modulus of CAFNs is approximately proportional to ρ_c^2, which in general agrees with the scaling relationship of the experimental results in literature [10]. **Table 3** lists the simulation results of the in-plane effective shear moduli of CAFNs and the experimental measurements for comparison. In experiments, the crosslinking density of CAFNs is dominated by the molar ratio of FLNA dimer to actin monomer, and it is reported that 0.2 μm long actin filament contains about 76 subunits of actin monomers[44]. Thus, the equivalent molar ratio of FLNA to actin in FE model can be obtained as $R_F = \rho_c / 380$. It is worth noting that the in-plane shear moduli of CAFNs obtained from simulations are slightly larger than those obtained from experiments. This is because it is difficult for us to perfectly match the crosslinking densities in simulations with those in experiments. In experiments, the molar ratio of FLNA dimer to actin monomer

22

corresponds to the amount of the FLNA dimer that has been added in, but some of them may be isolated. However, in computer simulations, every cross-linker is connected with actin filaments to contribute to the macro stiffness of the CAFNs.

(a)   (b)
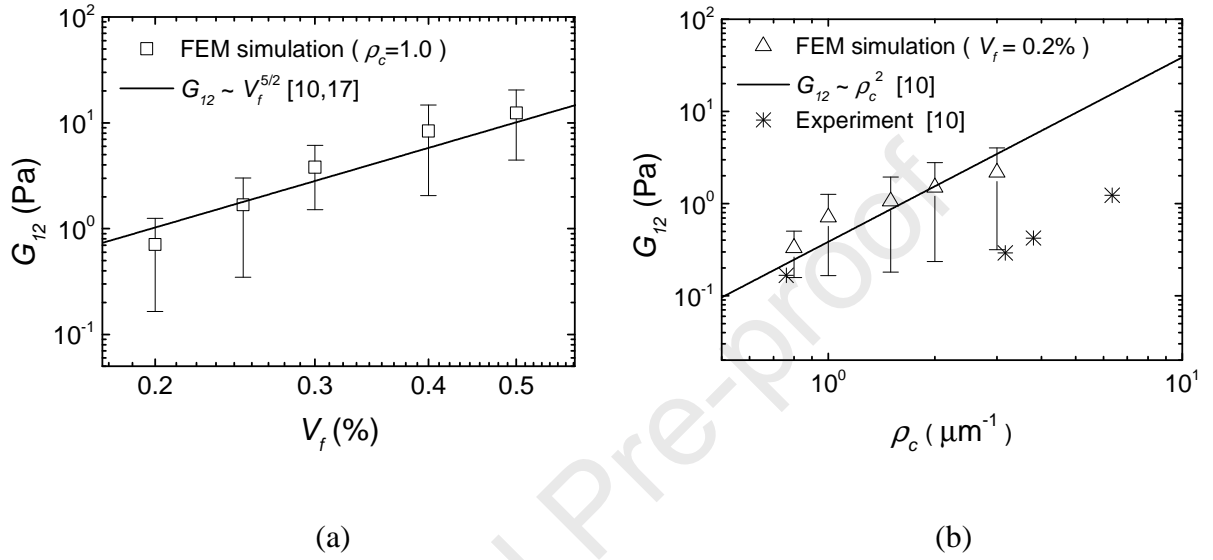
Fig. 5. The in-plane shear modulus of CAFNs, G_{12}, as a function of the actin filament volume fraction

(a) and the crosslinking density (b).
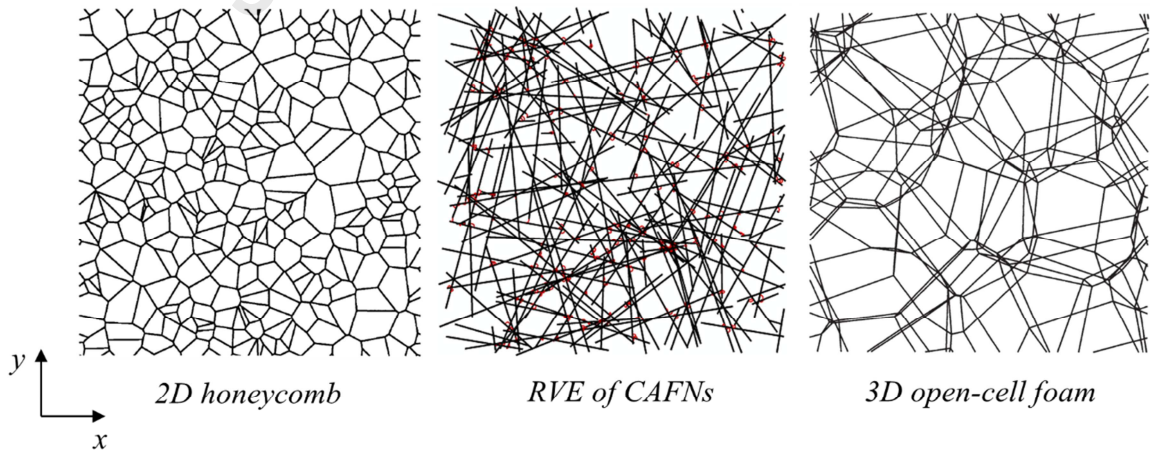
Fig. 6. The geometries of an undeformed random Voronoi honeycomb (2D) [63], an undeformed

random RVE of CAFNs (3D) and an undeformed random Voronoi open-cell foam (3D) [62].

Table 3

Comparison between the effective in-plane shear moduli of CAFNs obtained from experiments in literature and those obtained from simulations in this research.

Method	Volume fraction (%)	Mean length (μm)	Molar ratio (ABPs/actin)	G_{12} (Pa)	Ref.
Experiment	0.05	2.5 – 3.0	1:300	0.2	Goldmann et al. [68]
Experiment	0.05	2.0	1:100	0.2	Kasza et al. [15]
Experiment	0.05	2.0	1:100	0.1	Lee et al. [69]
Experiment	0.1	1.0	1:50	2	Kasza et al. [70]
Experiment	0.2	1.0 – 2.0	1:100	1 - 1.5	Gardel et al. [11]
Simulation	0.2	1.0	1:380	0.71	in this research
Simulation	0.2	1.0	1:190	1.50	in this research
Simulation	0.2	1.0	1:125	2.17	in this research

4. Dimensional analysis

In addition to the volume fraction of actin filament, V_f, and the crosslinking density, ρ_c, the elastic properties and deformation mechanisms of the component materials can also affect the stiffness of CAFNs. However, to the best of our knowledge, this aspect has not been well studied. Here, we explore how the in-plane shear modulus of CAFNs depends on the elastic properties and the deformation mechanisms of their components by dimensional analysis and numerical simulations, and thus identify their contributions to the stiffness of CAFNs.

It is reported that the elastic properties of CAFNs are bending dominated [13, 59] in small strain stage. However, the effect of the torsional deformation of cross-linkers on the stiffness of CAFNs has almost never been investigated. In this research, an L-shaped cantilever beam model as shown in **Fig. 7**, which takes the torsion and bending of FLNA as well as the bending of actin filament into consideration, is proposed to perform dimensional analysis on the shear deformation behaviour of CAFNs. In **Fig. 7**, *ABC* refers to the rod 2 segment of FLNA dimer with a length of $L_c = 0.04$ μm and it is in the *x-z* plane, *CD* refers to actin

24

filament (in the x direction) with a length of L_f, and P is a very small concentrated force applied in the y direction at point D. As the dimensional analysis is mainly focused on the qualitative analysis, the main part (BCD) of the L-shaped cantilever beam model is simply assumed to be perpendicular to the side face of RVE. Though actin filaments may be not always perpendicular to the side face of RVE, this just influences the coefficient parameter rather than the dimensional analysis conclusions. The Young's moduli of FLNA and actin filament are E_c and E_f, and the second moments of their cross-sectional areas are I_c and I_f, respectively.
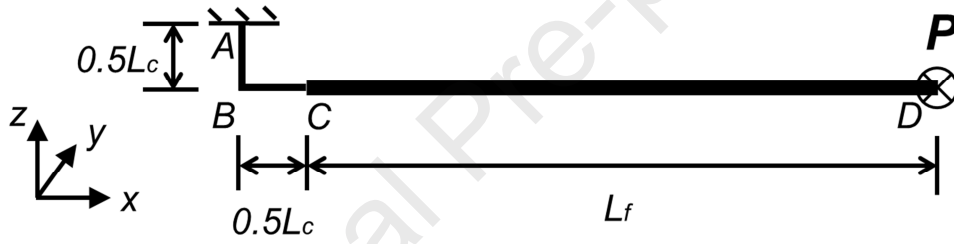
Fig. 7. The schematic diagram of an L-shaped cantilever beam model for dimension analysis. P is a small concentrated force applied in y direction at point D.

According to **Fig. 7**, when a concentrated force, P, is applied in the y direction at point D, the deflection in the y direction and the rotation about the z axis of point B are obtained as

$$y_B = \frac{P \cdot (0.5L_c)^3}{3E_c I_c}, \tag{10}$$

$$\theta_B = \frac{P \cdot (0.5L_c + L_f) \cdot 0.5L_c}{G_c I_{Pc}}, \tag{11}$$

where G_c is the shear modulus of FLNA, I_{Pc} is the second polar moment of inertia of FLNA.

25

The deflection in the y direction and the rotation about the z axis of point C can be obtained and given as

$$y_C = \frac{P \cdot (0.5 \cdot L_c)^3}{3E_c I_c} + \frac{PL_f \cdot (0.5L_c)^2}{2E_c I_c} + y_B + \theta_B \cdot 0.5L_c, \tag{12}$$

$$\theta_C = \frac{P \cdot (0.5L_c)^2}{2E_c I_c} + \frac{PL_f \cdot (0.5L_c)}{E_c I_c} + \theta_B. \tag{13}$$

Using superposition, the deflection of point D in the y direction is derived as

$$\begin{aligned}
y_D &= y_C + \theta_C L_f + \frac{PL_f^3}{3E_f I_f} \\
&= \frac{P \cdot (0.5L_c + L_f) \cdot 0.5L_c L_f}{G_c I_{Pc}} + \frac{P \cdot (0.5L_c)^2 L_f}{2E_c I_c} + \frac{PL_f^2 \cdot (0.5L_c)}{E_c I_c} + \\
&\quad \frac{P \cdot (0.5L_c)^3}{3E_c I_c} + \frac{PL_f \cdot (0.5L_c)^2}{2E_c I_c} + \frac{P \cdot (0.5L_c)^3}{3E_c I_c} + \frac{P \cdot (0.5L_c + L_f) \cdot (0.5L_c)^2}{G_c I_{Pc}} + \frac{PL_f^3}{3E_f I_f} \\
&= \frac{P \cdot (0.5L_c + L_f)^2 \cdot 0.5L_c}{G_c I_{Pc}} + \frac{2P \cdot (0.5L_c)^3}{3E_c I_c} + \frac{PL_f \cdot (0.5L_c)^2}{E_c I_c} + \frac{PL_f^2 \cdot (0.5L_c)}{E_c I_c} + \frac{PL_f^3}{3E_f I_f}
\end{aligned} \tag{14}$$

The bending stiffness of actin filament (*CD*), k_f, the bending stiffness of cross-linker (*AB* and *BC*), k_{cb}, and the torsion stiffness of cross-linker (*AB*), k_{ct}, are defined as

$$\begin{cases}
k_f = E_f I_f / L_f^3 = E_f \pi d_f^4 / (64 L_f^3) \\
k_{cb} = E_c I_c / (0.5L_c)^3 = E_c \pi d_c^4 / \left[64 \times (0.5L_c)^3 \right] , \\
k_{ct} = G_c I_{Pc} / (0.5L_c)^3 = G_c \pi d_c^4 / \left[32 \times (0.5L_c)^3 \right]
\end{cases} \tag{15}$$

where d_f and d_c are the diameters of the circular cross sections of actin filament and cross-linker respectively, L_f and L_c are the lengths of actin filament and cross-linker respectively. In addition, $I_{Pc} = 2I_c$, and $G_c = E_c / 2(1 + v_c)$ is the shear modulus for the cross-linker material, where v_c is the Poisson's ratio of the cross-linker. Thus, the effective shear strain of the crosslinked actin filament networks (CAFNs) can be scaled as

26

$$
\gamma = \frac{y_D}{0.5L_c + L_f}
$$

$$
= \frac{P \cdot (0.5L_c + L_f) \cdot 0.5L_c}{G_c I_{Pc}} + \frac{2P \cdot (0.5L_c)^3}{3E_c I_c \cdot (0.5L_c + L_f)} +
$$

$$
\frac{PL_f \cdot (0.5L_c)^2}{E_c I_c \cdot (0.5L_c + L_f)} + \frac{PL_f^2 \cdot (0.5L_c)}{E_c I_c \cdot (0.5L_c + L_f)} + \frac{PL_f^3}{3E_f I_f \cdot (0.5L_c + L_f)} \qquad , \qquad (16)
$$

$$
= \frac{P \cdot (0.5L_c + L_f) \cdot 0.5L_c}{\kappa_{ct} \cdot (0.5L_c)^3} + \frac{2P \cdot (0.5L_c)^3}{3\kappa_{cb} \cdot (0.5L_c)^3 \cdot (0.5L_c + L_f)} +
$$

$$
\frac{PL_f \cdot (0.5L_c)^2}{\kappa_{cb} \cdot (0.5L_c)^3 \cdot (0.5L_c + L_f)} + \frac{PL_f^2 \cdot (0.5L_c)}{\kappa_{cb} \cdot (0.5L_c)^3 \cdot (0.5L_c + L_f)} + \frac{PL_f^3}{3\kappa_f L_f^3 \cdot (0.5L_c + L_f)}
$$

To obtain the effective shear stress applied on the side face of the RVE, it is simply assumed that there are n actin filaments crossing each side face of the RVE model (**Fig. 1** (c)). In the RVE, actin filaments are randomly distributed, which means that they are in general not perpendicular to the side face of the RVE. But this does not influence the dimensional analysis conclusion as the dimensional analysis is mainly focused on qualitative analysis. By assuming P_i as the concentrated forces applied in the y direction at the ends of actin filaments which cross the side face of RVE, the effective shear force (F) applied on the side face of the RVE can be given as

$$
F = \sum_{i=1}^{n} P_i , \qquad (17)
$$

where n is the total number of actin filaments that cross one of the side faces of RVE.

Thus, the effective shear stress applied on one of the side faces of the RVE can be expressed as

$$
\tau = F/WH = \sum_{i=1}^{n} P_i \Big/ WH \quad , \qquad (18)
$$

where W and H are the side length and thickness of the RVE model, respectively.

27

The effective in-plane shear modulus of the RVE can thus be obtained, and given as

$$G_{12} = \frac{\tau}{\gamma}$$
$$= \frac{3(0.5L_c + L_f)\sum_{i=1}^{n} P_i}{WHP} \cdot \frac{k_{ct}k_{cb}k_f}{k_{ct}k_{cb} + k_f \cdot \left[3k_{cb}\cdot(0.5L_c + L_f)^2 + 2k_{ct}\cdot(0.5L_c)^2 + 3k_{ct}L_f\cdot(0.5L_c) + 3k_{ct}L_f^2\right]\Big/(0.5L_c)^2}$$

(19)

In this L-shaped cantilever beam model (**Fig. 7**), L_c refers to the total length of rod 2 segment in FLNA dimer (i.e., CDC' in **Fig. 3** (a)) which is reported to be 40 nm [49, 53]. L_f is the average length of actin filament segments between two neighbouring cross-linkers and given as

$$L_f = L_t/n_c \ ,$$

(20)

where L_t and n_c are the total length of actin filaments and the total number of cross-linkers in the RVE model, respectively. It is easy to find that L_f is the reciprocal of the crosslinking density ρ_c. According to Eq. (15), the bending stiffness k_{cb} (or k_f) depends on not only the Young's modulus of cross-linker (or actin filament), but also the length of cross-linker (or actin filament). The torsion stiffness of cross-linker, k_{ct}, depends on the Young's modulus, Poisson's ratio and length of the cross-linker. In order to explore either the cross-linkers or the actin filaments dominate the stiffness (i.e., G_{12}) of the CAFNs, we fix the Poisson's ratios of cross-linker and actin filament at 0.35, the volume fraction of actin filaments at 0.2%, and the crosslinking density at 1.0. As L_f can be obtained to be 1 μm according to Eq. (20), we have $\left[3k_{cb}\cdot(0.5L_c + L_f)^2 + 2k_{ct}\cdot(0.5L_c)^2 + 3k_{ct}L_f\cdot(0.5L_c) + 3k_{ct}L_f^2\right]\Big/(0.5L_c)^2 = 7803k_{cb} + 7652k_{ct}$.

In such a condition, the stiffnesses k_{ct}, k_{cb} and k_f only depend on E_c and E_f, respectively. By

28

noting $3L_c\left(0.5L_c+L_f\right)\sum_{i=1}^{n}P_i\Big/WHP$ as a constant coefficient parameter, λ, Eq. (19) can be rewritten as

$$G_{12} = \lambda k_{ct}k_{cb}k_f\Big/\left\{L_c\cdot\left[k_{ct}k_{cb}+k_f\cdot(7803k_{cb}+7652k_{ct})\right]\right\}. \tag{21}$$

As the cross-linkers have a circular cross-section and are made of an isotropic material, $G_c = E_c/2(1+v_c)$ and $I_{Pc} = 2I_c$, thus

$$k_{ct}=k_{cb}/(1+v_c). \tag{22}$$

A new symbol $k_c=k_{cb}=(1+v_c)k_{ct}$ is introduced to represent the amplitude of the bending stiffness of the cross-linkers, Eq. (21) can be rewritten as

$$G_{12} = \lambda k_c k_f\Big/[L_c\left(k_c+18186k_f\right)] \tag{23}$$

Thus, $k_c k_f\big/[L_c\left(k_c+18186k_f\right)]$ can be used to demonstrate how the shear modulus G_{12} of CAFNs depends on the stiffnesses of the cross-linkers and actin filaments. We respectively increase or reduce the Young's modulus of either the cross-linkers or the actin filaments by one or more orders, while fixing the Young's modulus of the others at the normal level. The different values of E_c , E_f, k_c and k_f used for discussion are listed in **Table 4**. In order to identify either k_c or k_f dominates the stiffness (i.e., G_{12}) of the CAFNs, the values of G_{12}/λ are obtained from Eq. (23) and plotted against k_c and k_f in **Fig. 8**.

Table 4

The values of the Young's moduli and bending stiffnesses of cross-linkers and actin filaments used for discussion in **Fig. 8**.

29

| V_f	ρ_c	E_c (Pa)	k_c (Nm^{-1})	E_f (Pa)	k_f (Nm^{-1})
0.2%	1.0	1.2×10^4	1.24×10^{-8}	2.3×10^6	7.28×10^{-11}
0.2%	1.0	1.2×10^5	1.24×10^{-7}	2.3×10^7	7.28×10^{-10}
0.2%	1.0	1.2×10^6	1.24×10^{-6}	2.3×10^8	7.28×10^{-9}
0.2%	1.0	1.2×10^7	1.24×10^{-5}	2.3×10^9	7.28×10^{-8}
0.2%	1.0	1.2×10^8	1.24×10^{-4}	2.3×10^{10}	7.28×10^{-7}
0.2%	1.0	1.2×10^9	1.24×10^{-3}	2.3×10^{11}	7.28×10^{-6}
0.2%	1.0	1.2×10^{10}	1.24×10^{-2}	2.3×10^{12}	7.28×10^{-5}

(a)

(b)
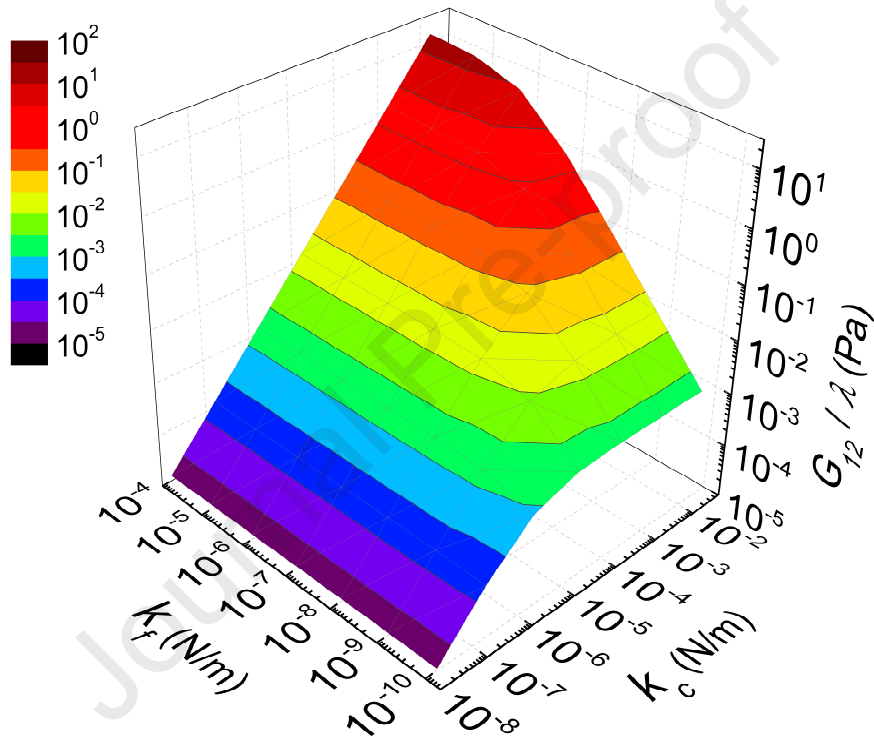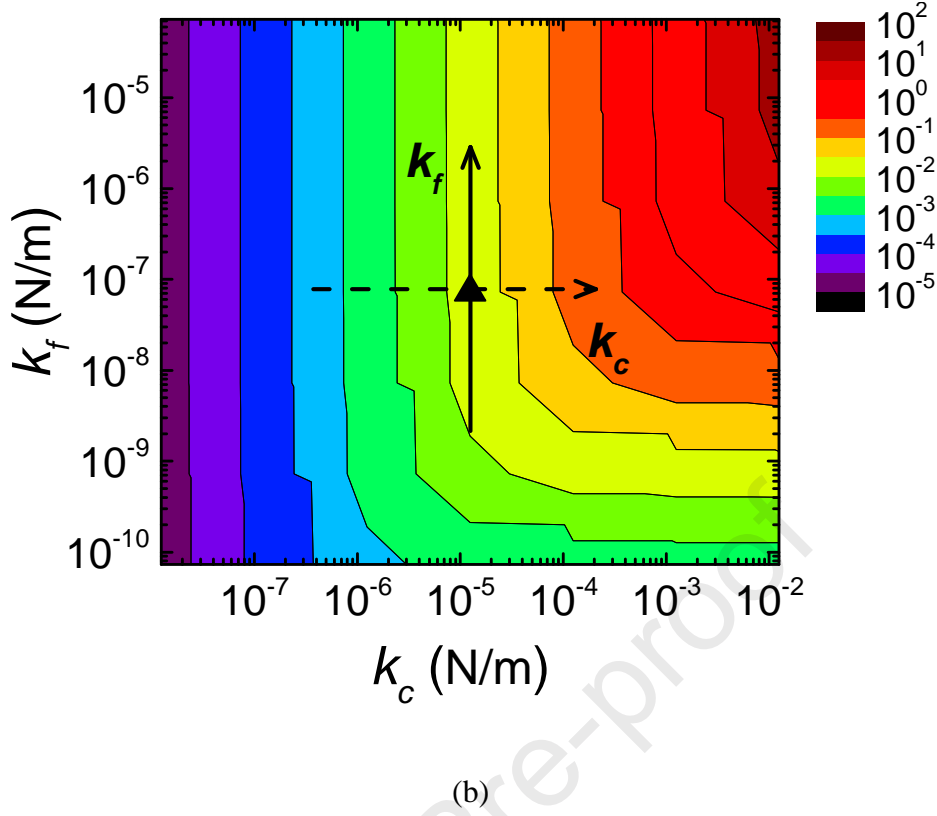
Fig. 8. (a) Dependences of G_{12}/λ on the bending stiffness k_c of FLNA and the bending

stiffness k_f of actin filaments when $V_f = 0.2\%$ and $\rho_c = 1.0$. (b) The plane isoline graphs of

G_{12}/λ against k_c and k_f when $V_f = 0.2\%$ and $\rho_c = 1.0$. The solid triangle represents the

combination of the normal stiffnesses of FLNA (i.e., $k_c = 1.24\times10^{-5}$ Nm^{-1}) and actin filament

(i.e., $k_f = 7.28\times10^{-8}$ Nm^{-1}). The arrow with the broken line indicates the increase of k_c, and

the arrow with the solid line indicates the increase of k_f.

According to Eq. (15), the normal bending stiffness is $k_{c0} = 1.24\times10^{-5}$ Nm^{-1} for cross-linkers

or $k_{f0} = 7.28\times10^{-8}$ Nm^{-1} for actin filaments. If k_f remains constant, G_{12}/λ exhibits almost a

linear relationship with k_c when $k_c \ll k_f$, then the gradient drops with the further increase of

k_c, and G_{12}/λ becomes a constant when $k_c \gg k_f$. On the other hand, if k_c remains constant,

31

G_{12} / λ slightly increases with k_f, but the gradient drops with k_f and becomes zero when $k_f \gg k_c$. This clearly indicates that the elastic properties of CAFNs are mainly dominated by its weaker part/component. The plane isoline graph of G_{12} / λ against k_c and k_f is shown in **Fig. 8** (b), and the normal condition point is marked by the solid triangle. According to the plane isoline graph, when k_f is fixed at k_{f0}, it is easy to find that the small deformation stiffness of CAFNs shows a linear relationship with k_c near the normal condition point. However, when k_c is fixed at k_{c0}, the small deformation stiffness of CAFNs is not sensitive to k_f near the normal condition point. This also suggests that the elastic properties of CAFNs are mainly dominated by FLNA in normal conditions.

In addition, the dependences of the in-plane shear modulus of CAFNs, G_{12}, on k_c and k_f are investigated by performing FEM simulations, and the simulation results are shown in **Fig. 9**. Considering the randomness of the RVE model, 100 models are simulated for each condition, and the statistical results (i.e., the mean results and error bars) of the 100 models are presented. It is noted that as the vertical axes are in log scale, the error bars look not symmetric about the mean values in the **Fig. 9**. In FEM simulations, the volume fraction of actin filaments and the crosslinking density are the same as those used in the dimensional analysis, i.e., $V_f = 0.2\%$ and $\rho_c = 1.0$. In **Fig. 9** (a), the bending stiffness of actin filament, k_f, is fixed at k_{f0} (i.e., 7.28×10^{-8} Nm^{-1}). In **Fig. 9** (b), the bending stiffness of FLNA, k_c, is fixed at k_{c0} (i.e., 1.24×10^{-5} Nm^{-1}). In addition, different values of k_f and k_c are applied in **Fig. 9** (c) and **Fig. 9** (d) respectively to further verify the dimensional analysis results. As can be seen in **Fig. 9**, the FEM simulation results of G_{12} agree well with the predictions of the dimensional analysis.

32

(a)

(b)

(c)

(d)
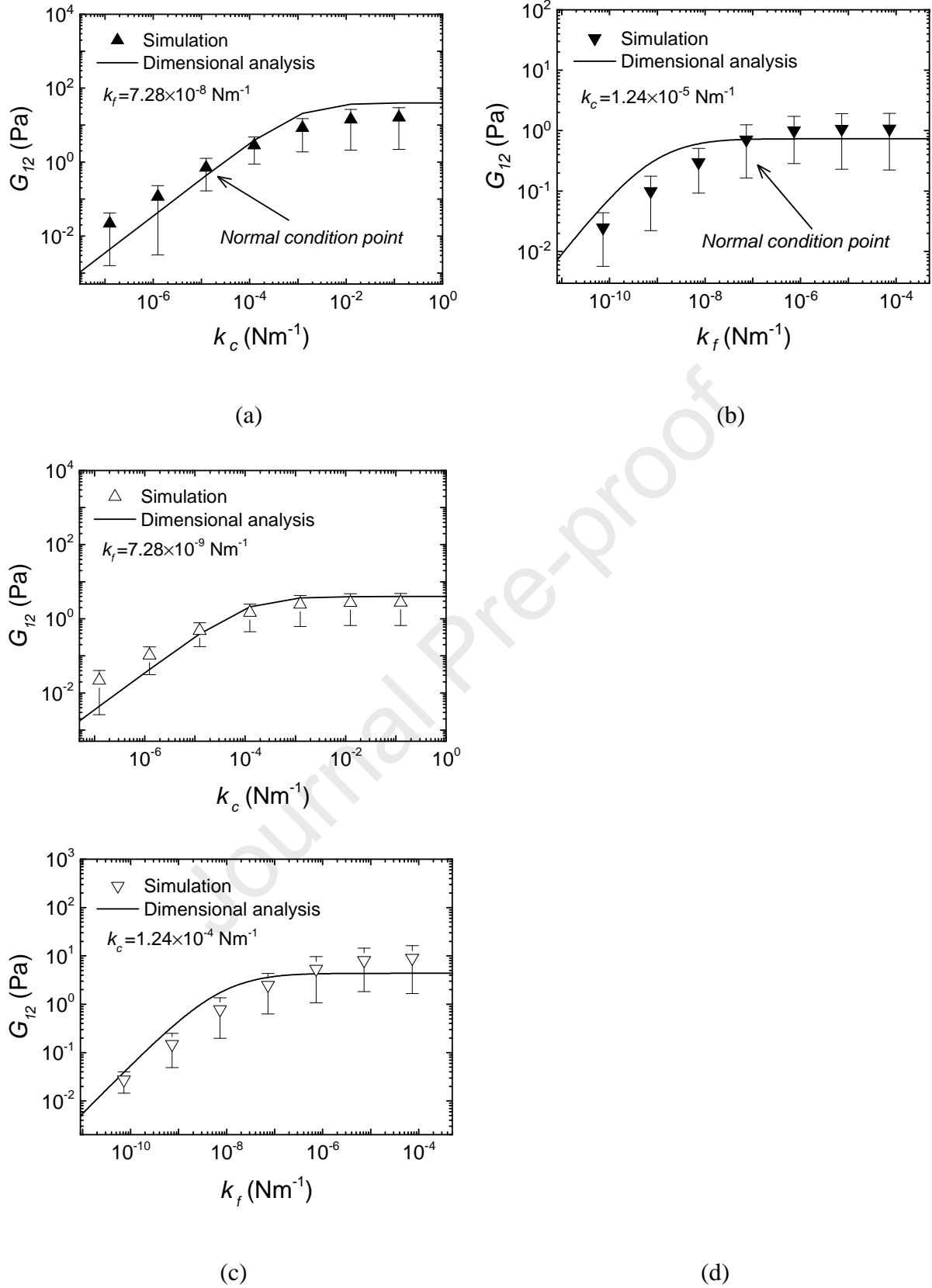
Fig. 9. Dependences of G_{12} on the bending stiffness of the FLNA (a) and (c) and the bending stiffness of the actin filament (b) and (d), where $V_f = 0.2\%$, $\rho_c = 1.0$. Simulation

33

results (solid triangles and open triangles) are compared with the dimensional analysis predictions (solid line). In (a) and (b), the bending stiffness of actin filament, k_f, and the bending stiffness of FLNA, k_c, are fixed at their normal condition values, respectively. To further verify the dimensional analysis results, the values of the bending stiffness of actin filament, k_f, and the bending stiffness of FLNA, k_c, are chosen to be different from their normal condition values in (c) and (d).

The Poisson's ratio is another important material parameter when performing simulations. Although it is reported that the Poisson's ratio of a viscoelastic solid could vary with time from 0.29 to 0.49 [71], the effects of the Poisson's ratios of actin filament and FLNA on the mechanical properties and the dominant deformation mechanism of CAFNs are found to be negligible, as demonstrated below. In order to probe the effects of the Poisson's ratios of actin filament (v_f) and FLNA (v_c) on the in-plane shear modulus of CAFNs, 100 random periodic CAFNs models with an actin filament volume fraction of 0.2% and a crosslinking density of 1.0 are simulated for numerical investigation. For simplicity, both the actin filament and FLNA are assumed to have the same Poisson's ratio. The effects of the Poisson's ratio of actin filament and FLNA on the in-plane shear modulus of the CAFNs are illustrated by the statistic results of 100 models shown in **Fig. 10**. As can be seen from **Fig. 10**, the in-plane shear modulus of CAFNs, G_{12}, decreases linearly and slightly (just about 2%) when the Poisson's ratio of the actin filament and FLNA increases from 0.35 to 0.499. The change in G_{12} is because both the torsion stiffnesses and the transverse shear stiffnesses of the actin filament and FLNA decrease with the increase of the Poisson's ratio. This indicates that the stiffness of the CAFNs is almost insensitive to the Poisson's ratios of actin filament and FLNA when they vary in the possible range from 0.29 to 0.499. In addition, two different combinations of the Poisson's ratios of actin filament and FLNA are used to further verify this conclusion. In the first combination, the Poisson's ratio of actin filament, v_f, is 0.29 with

the Poisson's ratio of FLNA, v_c, being 0.499. In the second combination, the Poisson's ratio of actin filament, v_f, is 0.499 with the Poisson's ratio of FLNA, v_c, being 0.29. Two groups of simulations are performed with these two combinations of the Poisson's ratios while all other parameters remain the same. The simulations results indicate that the difference between these two groups is just about 3.5%, confirming that the Poisson's ratios of actin filament and FLNA have negligible effects on the stiffness of CAFNs, and do not affect the dominant deformation mechanism.
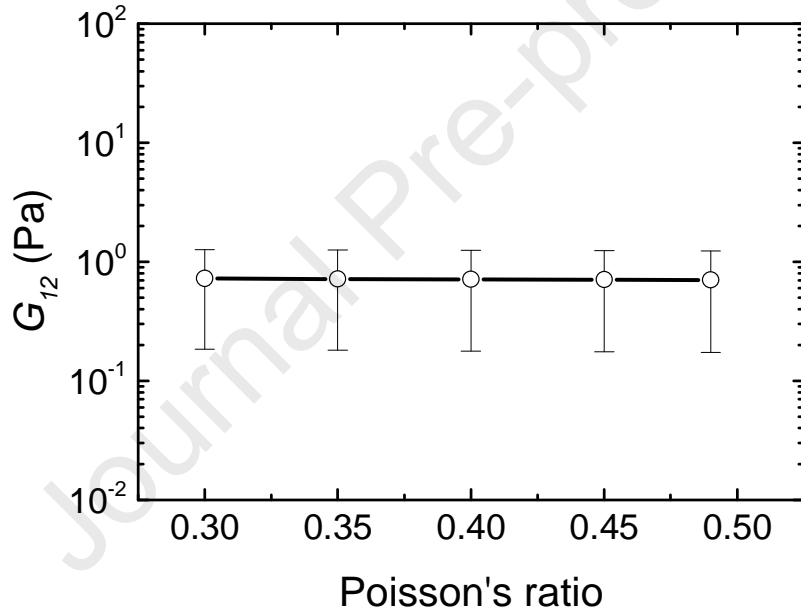
Fig. 10. Effects of the Poisson's ratio of actin filament and FLNA on the in-plane shear modulus of CAFNs. The statistic results are obtained from 100 random periodic CAFNs models, where $V_f = 0.2\%$, $\rho_c = 1.0$.

As the aspect ratios of the actin filaments and FLNA in our model are very large (larger than 10), the axial compression and transverse shear deformations of both the actin filaments and FLNA can fairly be ignored. To the best of our knowledge, the decoupled effects of the

35

bending and torsion deformations of actin filaments and FLNA on the stiffness (e.g., shear modulus) of CAFNs have never been studied before. In this research, four more different cases of testing simulations on the same 100 random RVE models are conducted to explore how the stiffness of CAFNs depends on the de-coupled bending and torsion deformations of actin filaments and FLNA, and to compare these results with that obtained from the normal condition (**Table 5**). In case-1, both the bending and torsion stiffnesses of FLNA are fixed at the normal condition while both the bending and torsion stiffnesses of actin filaments are five orders larger than those of FLNA. In this case, the deformations of the actin filaments can be ignored and the stiffness of CAFNs depends on only the deformation (i.e., bending and torsion) of FLNA. In case-2, the bending stiffness of FLNA is fixed at the normal condition, and the torsion stiffness of FLNA is five orders larger than its bending stiffness (this is realized by setting the Poisson's ratio of FLNA at -0.99999). In addition, both the bending and shear stiffnesses of the actin filaments are also five orders larger than the bending stiffness of FLNA. In this case, the stiffness of CAFNs depends on only the bending deformation of FLNA. In case-3, both the bending and torsion stiffnesses of the actin filaments are fixed at the normal condition, while both the bending and torsion stiffnesses of FLNA are five orders larger than those of the actin filaments. In this case, the stiffness of CAFNs depends only on the deformation (i.e., bending and torsion) of the actin filaments. In case-4, the bending stiffness of the actin filaments is fixed at the normal condition, while the torsion stiffness of the actin filaments is five orders larger than its bending stiffness. In addition, both the bending and shear stiffnesses of FLNA are also five orders larger than those of the actin filaments. In this case, the stiffness of CAFNs depends only on the bending deformation of the actin filaments.

Table 5 shows the simulation results of the shear modulus of the CAFNs for the four cases, and the result obtained from the normal condition is also provided for comparison. By

comparing the results of case-1 and case-3, it is very clear that the stiffness (or deformation) of CAFNs is dominated by FLNA (i.e., the cross-linkers), and that the bending and torsion deformations of the actin filaments have much smaller effects on the stiffness of CAFNs. By decoupling case-1 and case-2, it can be found that the torsion deformation of FLNA plays almost the same important role as the bending deformation of FLNA in determining the stiffness of CAFNs. The deflection of the CAFNs given by Eq. (14) can be approximately expressed as

$$
\begin{aligned}
\mathrm{y} &= \frac{P \cdot (0.5L_c + L_f)^2 \cdot 0.5L_c}{G_c I_{Pc}} + \frac{2P \cdot (0.5L_c)^3}{3E_c I_c} + \frac{PL_f \cdot (0.5L_c)^2}{E_c I_c} + \frac{PL_f^2 \cdot (0.5L_c)}{E_c I_c} + \frac{PL_f^3}{3E_f I_f} \\
&\approx \frac{P \cdot (0.5L_c + L_f)^2 \cdot 0.5L_c}{G_c I_{Pc}} + \frac{PL_f^2 \cdot (0.5L_c)}{E_c I_c} + \frac{PL_f^3}{3E_f I_f}
\end{aligned}
\tag{24}
$$

This is because $L_c \ll L_f$. Thus, the deflection (or stiffness) resulted from the torsion deformation of the cross-linker, $\dfrac{P \cdot (0.5L_c + L_f)^2 \cdot 0.5L_c}{G_c I_{Pc}}$, is almost the same as that resulted from the bending deformation of the cross-linker, i.e., $\dfrac{PL_f^2 \cdot (0.5L_c)}{E_c I_c}$. To the best of our knowledge, this is the first time to quantify the contribution of the torsion stiffness of FLNA (i.e., cross-linkers) to the stiffness of CAFNs.

In order to perform the sensitivity analysis in term of the geometry of crosslinkers, simulations are conducted on 100 CAFN models with straight crosslinkers, and the statistic results are given in **Table 5** for comparison. As can be seen, the mean shear modulus of CAFNs with straight crosslinkers has increased 18% compared to those with the "V" shaped crosslinkers. This is because straight crosslinkers are shorter and thus stiffer than the "V" shaped crosslinkers. The simulation results indicate that the stiffness of CAFNs with straight crosslinkers is also mainly determined by the stiffness of crosslinkers, and torsion

37

deformation of the straight cross-linkers plays a more significant role than their bending deformation in determining the stiffness of the CAFNs.

Table 5

Effects of the bending and torsion of actin filament and FLNA on the in-plane shear modulus (G_{12}) of CAFNs. Models with straight crosslinkers are also studied for comparison. The statistic results are obtained from 100 random periodic CAFNs models, where $V_f = 0.2\%$, $\rho_c = 1.0$.

Case	"V" shaped crosslinker		Straight crosslinker	
	G_{12} (Mean) Pa	Standard deviation	G_{12} (Mean) Pa	Standard deviation
Normal	0.7189	0.5381	0.8461	0.5818
1	1.3866	0.8221	1.5920	1.5676
2	2.6386	1.5979	34.2031	32.5497
3	15.2351	10.4626	14.3799	9.7474
4	20.5075	14.7296	18.3369	12.5196

5. Conclusions

In this paper, a novel random three-dimensional FEM model has been successfully developed to investigate the elastic properties of crosslinked actin filament networks. By performing FEM simulations, the effective in-plane Young's modulus, shear modulus and Poisson's ratio of the network are obtained. The simulation results show that the CAFNs are in-plane isotropic, and the scaling relationship between the in-plane shear modulus of CAFNs and the volume fraction of actin filaments agrees well with the experimentally measured

results ($G_{12} \sim V_f^{5/2}$) in literature. The in-plane shear modulus of CAFNs, G_{12}, is observed to scale with the square of the crosslinking density of CAFNs, i.e., $G_{12} \sim \rho_c^2$. By varying the actin filament volume fraction (via changing the concentration of actin) and crosslinking density (via altering the concentration of FLNA), the elastic properties of CAFNs could be optimized/tuned to meet the demanding requirements for distinct physiological functions (e.g., cell migration, cell growth and cell division). In addition, an L-shaped cantilever beam model has been developed for dimensional analysis on the shear modulus of CAFNs and for de-coupling the effects of bending and torsion deformation of FLNA (i.e., cross-linkers) on the stiffness of CAFNs. According to the dimensional analysis, the in-plane shear stiffness of CAFNs is mainly dominated by FLNA.   The FEM simulation results also confirm that the Poisson's ratios of actin filament and FLNA have negligible effects on the stiffness of CAFNs, and do not affect the dominant deformation mechanism. Four more cases of testing simulations on random RVE models are performed to de-couple the influences of the torsion deformation of cross-linkers and actin filaments on the stiffness of CAFNs by altering the torsion and bending stiffnesses of cross-linkers and actin filaments, respectively. The simulation results for the first time indicate that the torsion deformation of FLNA plays almost the same important role as the bending deformation of FLNA in determining the stiffness of CAFNs. The results obtained in this research can increase the understanding of the mechanical behaviors of CAFNs and help us to reveal the roles of CAFNs in different cell functions.

Acknowledgments

References

[1]   G. Salbreux, G. Charras, E. Paluch, Actin cortex mechanics and cellular morphogenesis, Trends in cell biology 22(10) (2012) 536-545.

[2]   C.D. Nobes, A. Hall, Rho, Rac, and Cdc42 GTPases regulate the assembly of multimolecular focal complexes associated with actin stress fibers, lamellipodia, and filopodia, Cell 81 (1995) 53-62.

[3]   M. Krause, A. Gautreau, Steering cell migration: lamellipodium dynamics and the regulation of directional persistence, Nat Rev Mol Cell Biol 15(9) (2014) 577-590.

[4]   K.H. Vining, D.J. Mooney, Mechanical forces direct stem cell behaviour in development and regeneration, Nat Rev Mol Cell Biol 18(12) (2017) 728-742.

[5]   Y.W. Heng, C.G. Koh, Actin cytoskeleton dynamics and the cell division cycle, The international journal of biochemistry & cell biology 42(10) (2010) 1622-1633.

[6]   C. Litschko, S. Brühmann, A. Csiszár, T. Stephana, V. Dimchev, J. Damiano-Guercio, A. Junemann, S. Körber, M. Winterhoff, B. Nordholz, N. Ramalingam, M. Peckham, K. Rottner, R. Merkel, J. Faixa, Functional integrity of the contractile actin cortex is safeguarded by multiple Diaphanous-related formins, Proceedings of the National Academy of Sciences of the United States of America 116(9) (2019) 3594-3603.

[7]   D.A. Fletcher, R.D. Mullins, Cell mechanics and the cytoskeleton, Nature 463(7280) (2010) 485-492.

[8]   L. Blanchoin, R. Boujemaa-Paterski, C. Sykes, J. Plastino, Actin dynamics, architecture, and mechanics in cell motility, Physiol Rev 94 (2014) 235-263.

[9]   P.A. Janmey, S. Hvidt, J. Kas, D. Lerche, A. Maggs, E. Sackmann, M. Schliwa, T.P. Stossel, The Mechanical Properties of Actin Gels, J Biol Chem 269 (1994) 32503-32513.

[10]   M.L. Gardel, J.H. Shin, F.C. MacKintosh, L. Mahadevan, P. Matsudaira, D.A. Weitz, Elastic Behavior of Cross-Linked and Bundled Actin Networks, Science 304 (2004) 1301-1305.

[11]   M.L. Gardel, F. Nakamura, J.H. Hartwig, J.C. Crocker, T.P. Stossel, D.A. Weitz, Prestressed F-actin networks cross-linked by hinged filamins replicate mechanical properties of cells, Proceedings of the National Academy of Sciences of the United States of America 103(6) (2006) 1762-1767.

[12]   B. Wagner, R. Tharmann, I. Haase, M. Fischer, A.R. Bausch, Cytoskeletal polymer networks: the molecular structure of cross-linkers determines macroscopic properties, Proceedings of the National Academy of Sciences of the United States of America 103(38) (2006) 13974-13978.

[13]   G.H. Koenderink, M. Atakhorrami, F.C. MacKintosh, C.F. Schmidt, High-frequency stress relaxation in semiflexible polymer solutions and networks, Physical review letters 96(13) (2006) 138307.

[14]   A. Sharma, A.J. Licup, K.A. Jansen, R. Rens, M. Sheinman, G.H. Koenderink, F.C. MacKintosh, Strain-controlled criticality governs the nonlinear mechanics of fibre networks, Nature Physics 12(6) (2016) 584-587.

[15]   K.E. Kasza, C.P. Broedersz, G.H. Koenderink, Y.C. Lin, W. Messner, E.A. Millman, F. Nakamura, T.P. Stossel, F.C. Mackintosh, D.A. Weitz, Actin filament length tunes elasticity of flexibly cross-linked actin networks, Biophysical journal 99(4) (2010) 1091-1100.

[16]   C. Storm, J.J. Pastore, F.C. MacKintosh, T.C. Lubensky, P.A. Janmey, Nonlinear elasticity in biological gels, Nature 435(7039) (2005) 191-194.

[17]   F.C. MacKintosh, J. Kas, P.A. Janmey, Elasticity of semiflexible biopolymer networks, Physical review letters 75(24) (1995) 4425-4428.

[18] T. van Dillen, P.R. Onck, E. Van der Giessen, Models for stiffening in cross-linked biopolymer networks: A comparative study, J Mech Phys Solids 56(6) (2008) 2240-2264.

[19] C.P. Broedersz, F.C. MacKintosh, Modeling semiflexible polymer networks, Rev Mod Phys 86(3) (2014) 995-1036.

[20] F. Meng, E.M. Terentjev, Nonlinear elasticity of semiflexible filament networks, Soft Matter 12(32) (2016) 6749-6756.

[21] J.S. Palmer, M.C. Boyce, Constitutive modeling of the stress-strain behavior of F-actin filament networks, Acta biomaterialia 4(3) (2008) 597-612.

[22] M.J. Unterberger, K.M. Schmoller, C. Wurm, A.R. Bausch, G.A. Holzapfel, Viscoelasticity of cross-linked actin networks: experimental tests, mechanical modeling and finite-element analysis, Acta biomaterialia 9(7) (2013) 7343-7353.

[23] H. López-Menéndez, J.F. Rodríguez, Microstructural model for cyclic hardening in F-actin networks crosslinked by α-actinin, J Mech Phys Solids 91 (2016) 28-39.

[24] D.A. Head, A.J. Levine, F.C. MacKintosh, Deformation of cross-linked semiflexible polymer networks, Physical review letters 91(10) (2003) 108102.

[25] J. Wilhelm, E. Frey, Elasticity of stiff polymer networks, Physical review letters 91(10) (2003) 108103.

[26] P.R. Onck, T. Koeman, T. van Dillen, E. van der Giessen, Alternative explanation of stiffening in cross-linked semiflexible networks, Physical review letters 95(17) (2005) 178102.

[27] A.R. Missel, M. Bai, W.S. Klug, A.J. Levine, Affine-nonaffine transition in networks of nematically ordered semiflexible polymers, Physical review. E, Statistical, nonlinear, and soft matter physics 82(4 Pt 1) (2010) 041907.

[28] X. Wei, Q. Zhu, J. Qian, Y. Lin, V.B. Shenoy, Response of biopolymer networks governed by the physical properties of cross-linking molecules, Soft Matter 12(9) (2016) 2537-2541.

[29] E.M. Huisman, T. van Dillen, P.R. Onck, E. Van der Giessen, Three-dimensional cross-linked F-actin networks: relation between network architecture and mechanical behavior, Physical review letters 99(20) (2007) 208103.

[30] C. Mohrdieck, F. Dalmas, E. Arzt, R. Tharmann, M.M. Claessens, A.R. Bausch, A. Roth, E. Sackmann, C.H. Schmitz, J. Curtis, W. Roos, S. Schulz, K. Uhrig, J.P. Spatz, Biomimetic models of the actin cytoskeleton, Small 3(6) (2007) 1015-1022.

[31] M. Bai, A.R. Missel, A.J. Levine, W.S. Klug, On the role of the filament length distribution in the mechanics of semiflexible networks, Acta biomaterialia 7(5) (2011) 2109-2118.

[32] C.P. Broedersz, X. Mao, T.C. Lubensky, F.C. MacKintosh, Criticality and isostaticity in fibre networks, Nat Phys 7(12) (2011) 983-988.

[33] C.J. Cyron, K.W. Müller, A.R. Bausch, W.A. Wall, Micromechanical simulations of biopolymer networks with finite elements, J Comput Phys 244 (2013) 236-251.

[34] K.M. Heidemann, A. Sharma, F. Rehfeldt, C.F. Schmidt, M. Wardetzky, Elasticity of 3D networks with rigid filaments and compliant crosslinks, Soft Matter 11(2) (2015) 343-354.

[35] S. Lin, X. Han, G.C.P. Tsui, D. Hui, L. Gu, Active stiffening of F-actin network dominated by structural transition of actin filaments into bundles, Composites Part B: Engineering 116 (2017) 377-381.

[36] T. Kim, W. Hwang, H. Lee, R.D. Kamm, Computational analysis of viscoelastic properties of crosslinked actin networks, PLoS computational biology 5(7) (2009) e1000439.

[37] D.A. Head, A.J. Levine, F.C. MacKintosh, Distinct regimes of elastic response and deformation modes of cross-linked cytoskeletal and semiflexible polymer networks, Physical review. E, Statistical, nonlinear, and soft matter physics 68(6 Pt 1) (2003) 061907.

[38] A. Sharma, M. Sheinman, K.M. Heidemann, F.C. MacKintosh, Elastic response of filamentous networks with compliant crosslinks, Physical review. E, Statistical, nonlinear, and soft matter physics 88(5) (2013) 052705.

[39] Y.H. Ma, H.X. Zhu, B. Su, G.K. Hu, R. Perks, The elasto-plastic behaviour of three-dimensional stochastic fibre networks with cross-linkers, J Mech Phys Solids 110 (2018) 155-172.

[40] F. Gittes, B. Mickey, J. Nettleton, J. Howard, Flexural rigidity of microtubules and Actin Filaments Measured from Thermal Fluctuations in Shape, J. Cell Biol 120(4) (1993) 923-934.

[41] H. Kojima, A. Ishuima, T. Yanagida, Direct measurement of stiffness of single actin filaments with and without tropomyosin by in vitro nanomanipulation, Proceedings of the National Academy of Sciences of the United States of America 91 (1994) 12962-12966.

[42] H. Isambert, P. Venier, A.C. Maggs, A. Fattoum, R. Kassab, D. Pantaloni, M.-F. Carlier, Flexibility of Actin Filaments Derived from Thermal Fluctuations, J Biol Chem 270(19) (1995) 11437-11444.

[43] M. Yamazaki, S. Furuike, T. Ito, Mechanical response of single filamin A (ABP-280) molecules and its role in the actin cytoskeleton, J Muscle Res Cell Motil 23 (2002) 525-534.

[44] J.L. Podolski, T.L. Steck, Length Distribution of F-actin in Dictyostelium discoideum, J Biol Chem 265 (1990) 1312-1318.

[45] F. Eghiaian, A. Rigato, S. Scheuring, Structural, mechanical, and dynamical variability of the actin cortex in living cells, Biophysical journal 108(6) (2015) 1330-1340.

[46] D. Bray, J.G. White, Cortical flow in animal cells, Science 239(4842) (1988) 883-888.

[47] A.G. Clark, K. Dierkes, E.K. Paluch, Monitoring actin cortex thickness in live cells, Biophysical journal 105(3) (2013) 570-580.

[48] P. Chugh, A.G. Clark, M.B. Smith, D.A.D. Cassani, K. Dierkes, A. Ragab, P.P. Roux, G. Charras, G. Salbreux, E.K. Paluch, Actin cortex architecture regulates cell surface tension, Nat Cell Biol 19(6) (2017) 689-697.

[49] B. Gong, J. Lin, X. Wei, J. Qian, Y. Lin, Cross-linked biopolymer networks with active motors: Mechanical response and intra-network transport, J Mech Phys Solids 127 (2019) 80-93.

[50] T.P. Stossel, J. Condeelis, L. Cooley, J.H. Hartwig, A. Noegel, M. Schleicher, S.S. Shapiro, Filamins as intergrators of cell mechanics and signalling, Nat Rev Mol Cell Biol 2 (2001) 138-145.

[51] M. Kawamura, K. Maruyama, Electron Microscopic Particle Length of F-Actin Polymerized in Vitro, J Biochem 67(3) (1970) 437-457.

[52] D. Sept, J. Xu, T.D. Pollard, J.A. McCammon, Annealing Accounts for the Length of Actin Filaments Formed by Spontaneous Polymerization, Biophysical journal 77 (1999) 2911-2919.

[53] S. Burlacu, P.A. Janmey, J. Borejdo, Distribution of actin filament lengths measured by fluorescence microscopy, Am J Physiol Cell Physiol 262(3) (1992) C569-C577.

[54] F. Nakamura, T.M. Osborn, C.A. Hartemink, J.H. Hartwig, T.P. Stossel, Structural basis of filamin A functions, J Cell Biol 179(5) (2007) 1011-1025.

[55] F.G. Schmidt, F. Ziemann, E. Sackmann, Shear field mapping in actin networks by using magnetic tweezers, Eur Biophys J. 24 (1996) 348-353.

[56] Y. Tseng, B.W. Schafer, S.C. Almo, D. Wirtz, Functional synergy of actin filament cross-linking proteins, J Biol Chem 277(28) (2002) 25609-25616.

[57] S. Furuike, T. Ito, M. Yamazaki, Mechanical unfolding of single filamin A (ABP-280) molecules detected by actomic force microscopy, FEBS Letters 498 (2001) 72-75.

[58] A.J. Ehrlicher, F. Nakamura, J.H. Hartwig, D.A. Weitz, T.P. Stossel, Mechanical strain in actin networks regulates FilGAP and integrin binding to filamin A, Nature 478(7368) (2011) 260-263.

[59] F. Nakamura, T.P. Stossel, J.H. Hartwig, The filamins: Organizers of cell structure and function, Cell Adhesion & Migration 5(2) (2011) 160-169.

[60] K.M. Schmoller, O. Lieleg, A.R. Bausch, Structural and viscoelastic properties of actin/filamin networks: cross-linked versus bundled networks, Biophysical journal 97(1) (2009) 83-89.

[61] O. Lieleg, M.M.A.E. Claessens, A.R. Bausch, Structure and dynamics of cross-linked actin networks, Soft Matter 6(2) (2010) 218-225.

[62] H.X. Zhu, J.R. Hobdell, A.H. Windle, Effects of cell irregularity on the elastic properties of open-cell foams, Acta Mater 48 (2000) 4893-4900.

[63] H.X. Zhu, J.R. Hobdell, A.H. Windle, Effects of cell irregularity on the elastic properties of 2D Voronoi honeycombs, J Mech Phys Solids 49(4) (2001) 857-870.

[64] H.X. Zhu, Size-dependent elastic properties of micro- and nano-honeycombs, J Mech Phys Solids 58(5) (2010) 696-709.

[65] H.X. Zhu, L.B. Yan, R. Zhang, X.M. Qiu, Size-dependent and tunable elastic properties of hierarchical honeycombs with regular square and equilateral triangular cells, Acta Mater 60(12) (2012) 4927-4939.

[66] J.J. Chiu, S. Chien, Effects of Disturbed Flow on Vascular Endothelium: Pathophysiological Basis and Clinical Perspectives, Physiol Rev 91(1) (2011) 327-387.

[67] Y.C. Lin, N.Y. Yao, C.P. Broedersz, H. Herrmann, F.C. Mackintosh, D.A. Weitz, Origins of elasticity in intermediate filament networks, Physical review letters 104(5) (2010) 058101.

[68] W.H. Goldmann, M. Tempel, I. Spencer, G. Isenberg, R.M. Ezzell, Viscoelasticity of actin-gelsolin networks in the presence of filamin, Eur. J. Biochem. 246 (1997) 373-379.

[69] H. Lee, J.M. Ferrer, F. Nakamura, M.J. Lang, R.D. Kamm, Passive and active microrheology for cross-linked F-actin networks in vitro, Acta biomaterialia 6(4) (2010) 1207-1218.

[70] K.E. Kasza, A.C. Rowat, J. Liu, T.E. Angelini, C.P. Brangwynne, G.H. Koenderink, D.A. Weitz, The cell as a material, Current opinion in cell biology 19(1) (2007) 101-107.

[71] R.S. Lakes, A. Wineman, On Poisson's ratio in linearly viscoelastic solids, J Elasticity 85 (2006) 45-63.

10th March 2020

All authors have approved the submission of this paper.

Yours sincerely,

Dr Hanxing Zhu

School of Engineering, Cardiff University

Cardiff CF24 3AA, UK

Email: zhuh3@cf.ac.uk

Tel: 0044 29 20874824

10th March 2020

We claim that there is no conflict of interest.

Yours sincerely,

Dr Hanxing Zhu

School of Engineering, Cardiff University

Cardiff CF24 3AA, UK

Email: zhuh3@cf.ac.uk

Tel: 0044 29 20874824